International Journal of Applied Earth Observation and Geoinformation 118 (2023) 103275

Contents lists available at ScienceDirect

International Journal of Applied Earth Observation and Geoinformation

journal homepage: www.elsevier.com/locate/jag

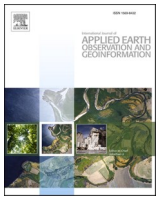

Forest total and component biomass retrieval via GA-SVR algorithm and quad-polarimetric SAR data

Jianmin Shi [a,1], Wangfei Zhang [a,*,1], Armando Marino [b], Peng Zeng [c], Yongjie Ji [d], Han Zhao [a], Guoran Huang [a], Mengjin Wang [a]

[a] College of Forestry, Southwest Forestry University, Kunming 650224, China
[b] Biological and Environmental Sciences, The University of Stirling, Stirling FK9 4LA, UK
[c] Yunnan Forest Nature Center, Kunming 650225, China
[d] School of Geography and Ecotourism, Southwest Forestry University, Kunming 650224, China

ARTICLE INFO

Keywords:
GA-SVR
Forest total and component AGB
Wavelength
Polarimetric SAR

ABSTRACT

A reliable evaluation of biomass is a vital prerequisite for realizing the international goal of "emission peak and carbon neutrality". It is critical to estimate the components of forest biomass, for ecosystem management. Additionally, working on components we may solve the saturation problems in AGB estimation using remote sensing features. In our previous works we proposed GA-SVR (Genetic algorithms and support vector regression) algorithm with polarimetric SAR (Synthetic Aperture Rader) to retrieve total forest Above Ground Biomass (AGB) estimation in our previous works, however, the potential of GA-SVR algorithm applied in component AGB estimation especially using combination of multi-frequency polarimetric SAR features deserves further exploration. In this study, we use quad-polarimetric SAR data at C- and L- bands, extracting the backscatter coefficients and polarimetric features derived from four polarization decomposition methods (Yamaguchi 3-component decomposition, Freeman 2-component decomposition, H/A/alpha decomposition, and TSVM decomposition) as the input to the GA-SVR for forest component AGB estimation. The effectiveness of 66 polarimetric features derived from C-, L-band at each test site was evaluated for forest component AGB prediction at two test sites. The outcomes demonstrated that the GA-SVR attained high estimation accuracy according to the values of coefficient of determination R^2, root mean square error, relative root mean square error, mean deviation, mean absolute deviation, mean percentage error, and mean absolute percentage error. The highest attained values of them were 0.77, 1.01 Mg/ha, 23.02%, −0.07 Mg/ha, 0.71 Mg/ha, 0.15%, and 18.42%, respectively. The study reconfirmed the robustness of GA-SVR algorithm and effectiveness of polarimetric SAR features extracted from four decomposition methods for forest total and AGB estimation. It also revealed that the capability of combining C-band L-band SAR polarimetric features for improving forest total and component AGB relies on the difference of forest structures.

1. Introduction

Forest biomass is a crucial measure for determining how well forests can absorb carbon dioxide and identify potential carbon sinks. It is a crucial indicator of carbon sequestration as well (Hayashi et al., 2019). Moreover, knowledge of the biomass distribution at each component of the forest, such as dry wood, bark, branches, and leaves AGBs (Above Ground Biomass), is also significant for assessing the productivity of forest ecosystems and improving refinement of forest resource surveys, which in turn improve the efficiency of forest planning and management (Lambert et al., 2005; Tsui et al., 2012). Meanwhile, Global carbon sink monitoring is the key to achieve the goals of peak carbon emissions and carbon neutrality ('Double Carbon'), and obtaining high-precision estimations of forest total and component AGB play a critical role to achieve the 'Double Carbon' goals.

Remote sensing (RS) technology provides the capability to capture the distribution, structure, and dynamics of forest resources on the ground at various geographical scales quickly, precisely, and timely,

* Corresponding author.
E-mail address: zhangwf@swfu.edu.cn (W. Zhang).
[1] These authors contributed to the work equally and should be regarded as co-first authors.

https://doi.org/10.1016/j.jag.2023.103275
Received 12 September 2022; Received in revised form 4 March 2023; Accepted 20 March 2023
Available online 14 April 2023

offering a strong scientific foundation for forest AGB monitoring (Astola et al., 2019; Gao et al., 2018; Zhao et al., 2016). RS is acknowledged as the only tool that can provide global spatially explicit estimates of forest AGB. Avitabile et al., (2016) proposed an approach to fuse maps with potential for combing individual AGB maps into a global map, such as GEO-CARBON map. However, this approach is insufficiently constrained in regions where in situ or other reference datasets are unavailable.

As different sensors 'see' different part of the forest, RS datasets involved in forest AGB retrieval include optical (multispectral, hyperspectral, etc.) data (Brovkina et al., 2017; Gibbs et al., 2007), synthetic aperture radar (SAR) data (Cartus and Santoro, 2019; Englhart et al., 2011; Hayashi et al., 2019), and light detection and ranging (LiDAR) data (Banskota et al., 2011; Tsui et al., 2012). Optical RS datasets are well suited to acquire forest top horizontal information like canopy cover, community type, etc. However, it suffers from an inability to penetrate through layers of vegetation to capture the vertical information of the forest. Meanwhile, accurate forest AGB retrieval depends on the availability of measures that capture both horizontal and vertical forest structure. Forest AGB retrieval using optical datasets have been demonstrated to saturated at relatively low AGB densities (Kellndorfer et al., 2004; Lu et al., 2016; Duncanson et al., 2022). LiDAR measures forest structure both in the horizontal dimension and vertical dimension and the Forest stand AGB derived from LiDAR has an accuracy similar to, or even better than ground measured values. However, the small area covered by airborne LiDAR sensor is a significant hindrance for large scale forest AGB inventories (Balzter et al.2007; Lu et al.,2016). Spaceborne LiDAR – ICESat GLAS-2 or GEDI is now available for regional- to global-scale applications, but it is impossible for direct wall-to-wall AGB mapping due to the spatially discrete characteristics (Lu et al.,2016; Xi et al.,2022; Duncanson et al.,2022). Moreover, both passive optical datasets or active Lidar datasets suffers dependence on weather conditions (not available during cloudy or rainy weather).

In comparison, synthetic aperture radar (SAR) sensor with all-weather and wall-to-wall monitoring capability has been demonstrated great potential for forest AGB retrieval. SAR backscatter signal (Santoro et al., 2006; Santoro et al., 2009; Sandberg et al.,2011), polarimetric information via polarimetric SAR (PolSAR) technology (Garestier et al.,2009; Chowdhury et al.,2013), interferometric coherence and phase via interferometric SAR (InSAR) (Santoro et al., 2002), polarimetric interferometric SAR (PoInSAR) (Cloude and Papathanassiou, 1998, 2003; Cloude, 2009; Liao et al.,2019), and coherence tomography and polarization coherence tomography (TomoSAR) technologies (Tebaldini, 2010; Tebaldini and Rocca, 2011; Yue et al., 2011; Blomberg et al.,2018; Cazcarra-Bes et al.,2017) were involved in forest AGB or forest height estimation. The effect of wavelength-dependent penetration depth into the forest scene is known to be large, and SAR sensors operating at long-wavelength like P-band have been proved to be more sensitive to forest AGB than at higher frequencies (X-, C-, S- and L-bands). Additionally, acquisitions displayed high temporal coherence between passes separated by several weeks and then allowing the use of InSAR, Pol-InSAR, and TomoSAR to estimate forest AGB by repeat-InSAR datasets. However, P-band SAR datasets are only available with airborne acquisition currently and limit their application in regional- and global-scale application. The urgent need for accurate forest AGB retrieval and the lack of any current space systems operating at P-band propelled the BIOMASS mission proposed by the European Space Agency (ESA) (Sandberg et al., 2011; Le Toan et al., 2011; Quegan et al., 2019). Unfortunately, the BIOMASS mission will only acquire data over tropical and subtropical regions due to the International Telecommunication Union-Radiocommunications restrictions over North America and Europe. However, L-band spaceborne SAR data, having different sensitivities for forest structure and forest AGB lower than 100 Mg/ha (Yu and Saatchi, 2016) will have a new mission with freely available data, known as NASA-ISRO SAR (NISAR) is scheduled to be launched in 2023 and works together with BIOMASS for global forest AGB mapping (Rosen et al., 2016; Yu and Saatchi, 2016).

Although the SAR backscatter of C-, and X-band is limited to retrieval higher AGB values, several previous researches determined that the SAR signals operated at higher frequencies has higher AGB estimation accuracy with lower variance at low forest AGB area than that estimated by lower frequencies (Englhart et al., 2011; Ji et al., 2021; Zeng et al.,2022). They also demonstrated the potential of combining L-band with X-/C-band to improve forest AGB estimation accuracy (Englhart et al., 2011; Cartus et al., 2019) Meanwhile, Polarimetric SAR data at various frequencies was found to have a significant potential for assessing forest AGB because of its sensitivity to the geometric characteristics, shape, and direction of the scattering objects (Chowdhury et al., 2013; Le Toan et al., 1992; Luckman et al., 1997). Quad polarimetric SAR datasets comprising of HH, HV, VH, and VV polarization channels express the polarization state changes in the received microwave caused mainly by the forest scatters' structures (Chowdhury et al., 2013). The characterization of quad polarimetric images revealed their potential for improving forest AGB assessment. Forest AGB estimation has been significantly improved by using polarimetric coherence and polarimetric phase computed from quad polarimetric SAR data. Several polarimetric decomposition features have been proved having high correlation with forest height, forest stem volume, and forest AGB as well (Chowdhury et al., 2013; Ji et al., 2021; Zeng et al., 2022).

Despite the fact that the work listed above demonstrated a huge potential of polarimetric features to encapsulate forest biophysical parameters, fewer papers have yet looked into the use of a combination of C- and L-band polarimetric features to estimate forest AGB, particularly for component AGB (Ji et al., 2021; Tsui et al., 2012; Zeng et al., 2022). Noticeably, previous studies mostly considered polarimetric decomposition features extracted from Freeman-Durden 3 components decomposition, H/A/alpha decomposition, and Yamaguchi 4 components decomposition theories (Kobayashi et al., 2012; Chowdhury et al., 2013). Despite the advancements made in forest AGB study utilizing these polarimetric features, less attention was been paid to polarimetric features extracted from other decompositions, such as arget scattering vector model (TSVM) (Chowdhury et al., 2013; Omar et al., 2017; Zeng et al., 2022). The combination of X- and L- band for AGB estimation in Kalimatan also confirmed the joint use of two frequencies SAR data resulting in estimation accuracy improvement (Englhart et al., 2011). The studies of Zeng et al. (2022) and Wei et al. (2020) explored the potential of polarimetric features extracted from Freeman-Durden 2 components decomposition (Freeman2), Yamaguchi 3 components decomposition (Yamaguchi3), and TSVM for total or component AGB estimation. These features were found to outperform traditional polarimetric features especially for canopy AGB retrieval. Since each frequency and polarization channel sense different aspects of forest structure, the use of multi-frequency polarimetric SAR allows us to monitor the dynamics of forest resources from multiple dimensions, raising the saturation point for the inversion of forest AGB.

Designing a proper algorithm to create AGB estimation models is just as important in the task of forest AGB modeling as choosing the right RS data. In recent decades, nonparametric models like support vector regression (SVR), k-nearest neighbor (KNN), and random forest (RF) have been acknowledged and used often in forest AGB estimation (Englhart et al., 2011; Gao et al., 2018; Lu, 2006;). Among them, SVR became an important approach for both low and high forest AGB inversion, thanks to the capability of producing relatively high estimation accuracy by dealing with a relatively small training sample to solve both linear and nonlinear problems. Despite the SVR good performance of SVR, the accuracy of its estimation is greatly influenced by the optimization of the model's input RS data and its model parameters (Santi et al., 2020; Gao et al., 2018; Ji et al., 2021). Ji et al. (2021) suggested a GA-SVR algorithm, which simultaneously optimizes the incoming RS features and model parameters, as a new solution for forest biomass estimation. It was reported that forest AGB retrieval accuracy could be improved when combining C-, L- band SAR data (Ji et al.,2021).

Table 1
The Information of the Acquired SAR data.

Test site	Band	Date	Angle of incidence (°)	Range (m)	Azimuth (m)	Mode	Sensor
Yiliang	C-	2018–05-18	39.1	2.248	5.120	QPSI	GF-3
	L-	2016–04-22	33.9	2.86	3.21	HBQ	PALSAR-2/ ALOS-2
Genhe	C-	2013–08-20	37.4	4.96	4.73	FQP	RADARSAT-2
	L-	2014–08-29	36.52	2.86	2.64	HBQ	PALSAR-2/ ALOS-2

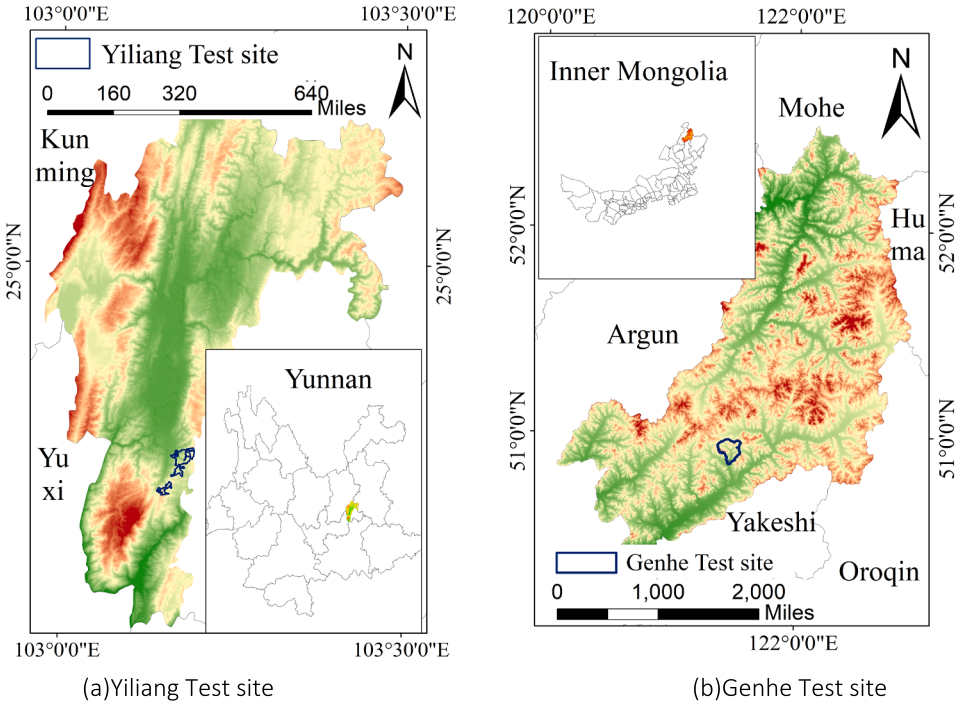

Fig. 1. Overview of the test sites.

It is well known that forest AGB estimation is tree-species dependent, site-dependent, and forest structure-dependent, which also relates with saturation problems hindering the AGB retrieval. Polarimetric features, considering the structure characterizations like direction and shape of the scatterers in forest scenes may have the potential to select the characterizations which can reflect the different scattering mechanisms. This can be achieved by a suitable inversion algorithm for feature optimization and applied in forest component AGB estimation. The

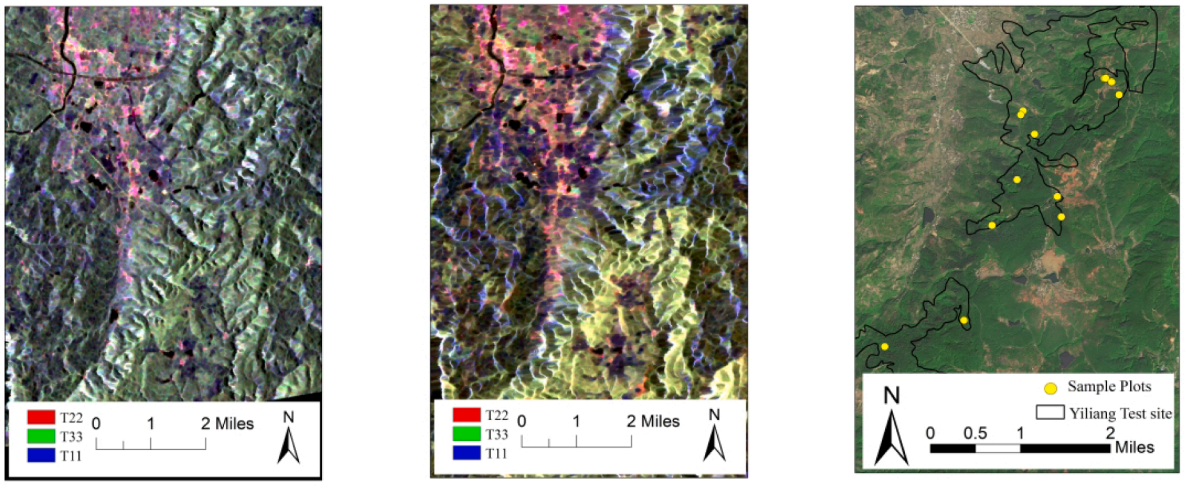

Fig. 2. SAR Images and filed collected samples of Yiliang test site, $R = T_{22} = |S_{hh} + S_{vv}|^2$, $G = T_{33} = |S_{hv}|^2$, and $B = T_{11} = |S_{hh} - S_{vv}|^2$, in the image are elements derived from the polarization coherence matrix $\boldsymbol{T}$, respectively.

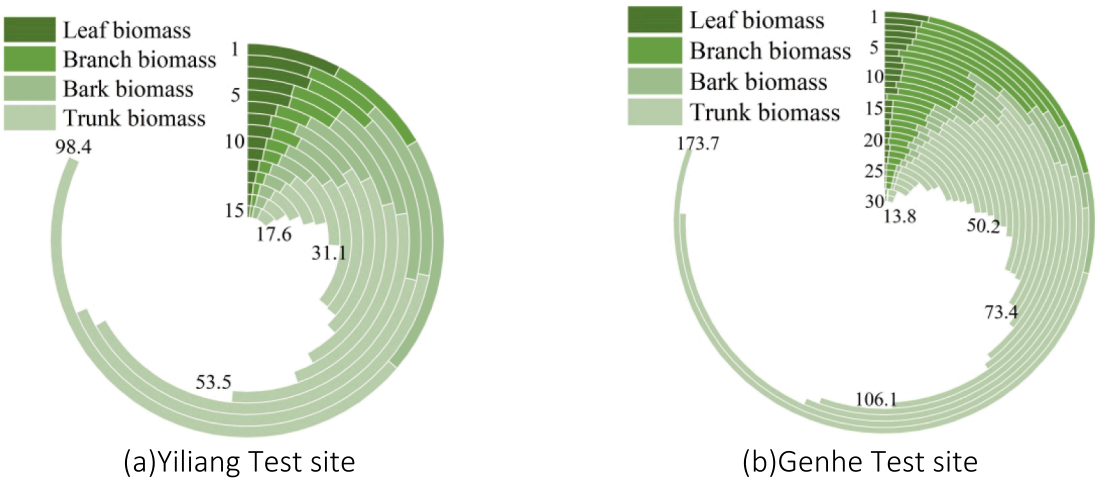

Fig. 3. The total and component forest AGB values (Mg/ha) of two test sites.

result from each component in forest scene can help researchers understand the signal coming for polarimetric features. Considering the potential of GA-SVR applied in component forest AGB at different test sites with different AGB levels is not fully explored, This study has the following objectives: 1) To find the optimal forest total and component AGB prediction performance using polarimetric features extracted from H/A/alpha decomposition, Freeman2, Yamaguchi3, and TSVM at C-, L-band; 2) To examine the potential of GA-SVR algorithm under the diversity of SAR data and test sites with different dominant tree species; 3) To test whether combination of C-, L- band SAR data can be used to improve forest total and component AGB estimation accuracy and saturation point.

2. Test sites and data sets

In this study we used data from two forest locations representing two important forest ecosystems: the boreal and subtropical with two very distinct dominating tree species and topographic features. Square sample plots were inventoried for two test sites for building the model and validating the results. Table 1 lists the C- and L- bands polarimetric SAR datasets available at each test site.

2.1. Yiliang test site

Yiliang test site is located in the Xiaoshao branch (24°39′~24°54′N; 103°02′~103°12′ E, Fig. 1 (a) of the Garden Forestry Farm in Yiliang County, Kunming City, Yunnan Province, Southwest of China. It represents typical subtropical forest system in southwest of China. It is an ancient woodland with an average AGB of 60 Mg/ha and maximum AGB less than 200 Mg/ha. Coniferous tree species such as Huashan pines (*Pinus armandii Franch*) and Yunnan pines (*Pinus yunnanensis*) are dominant in the forest. Yiliang County has a subtropical-plateau mountain monsoon climate at low latitudes with average annual temperatures around 16.3℃ and average annual precipitation of 912.2 mm. The slope in the test site ranges from 0° to 30° and with an elevation ranging from 1300 to 2500 m above mean sea level.

A scene of C- band Gaofen-3 (GF-3) quad-polarimetric image with Stripmap-1 mode and a scene of L-band full polarimetric ALOS-2 PALSAR-2 (Advanced Land Observing Satellite, Phase Array type L-band Synthetic Aperture Radar) data were collected at Yiliang test site for total and component forest AGB inversion. Fig. 2 (a) shows the GF-3 Pauli RGB image of the May 2018 acquisition. In Fig. 2 (b), ALOS-2 PALSAR-2 Pauli RGB acquired in April 2016 is shown and in Fig. 2 (c) the associate collected sample plot distribution is shown with Google Earth images as background. The coverage of Xiaoshao branch is indicated by the black boundary in Fig. 1 (c). Fig. 3 (a) shows the

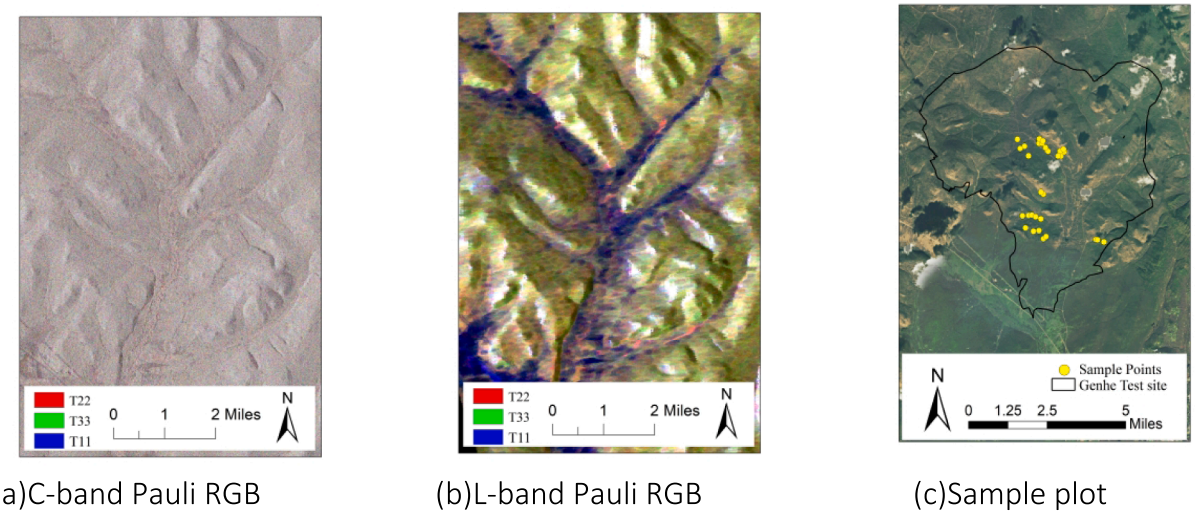

Fig. 4. SAR Images and filed collected samples of Genhe test site.

distribution of total and component AGB values for Yiliang test site.

2.2. Genhe test site

Genhe Test site is located in the Genhe City and within the Genhe national scientific field observing station for forest ecosystem (50°20′-52°30′N; 120°12-122°55′E, Fig. 1 (b)). Genhe is located in the northeast of Hulunbuir League, Northeast of China. It is covered with a boreal forest with dominated coniferous tree species of Xing'an larch (*Larix gmelinii*) and white birch (*Betula platyphylla*). It is an ancient woodland with a mean forest AGB of 78 Mg/ha, maximum forest AGB is less than 300 Mg/ha. The region has a cold temperate continental monsoon climate with an average annual temperature of −5.4 °C and 450 ~ 500 mm of annual precipitation. The elevation here ranges from 810 m to 1116 m beyond mean sea level with more than 80% areas are with a 15°slope and a height difference less than 300 m.

For this site, a scene of C- band Radarsat-2 image, a stripmap full polarimetric data obtained with a 37.4° incidence angle from a descending orbit in August 2013, and a scene of L-band ALOS-2 PALSAR-2 image, a High-Sensitive full polarimetric data obtained with a 36.52° incidence angle from a descending orbit in August 2014, have been investigated. Fig. 4 (a) shows the Radarsat-2 Pauli RGB image. In Fig. 4 (b), ALOS-2 PALSAR-2 Pauli RGB is shown and in Fig. 4 (c) the associate 30 collected sample plots are shown with Google Earth images as background with yellow points. The area of Genhe station is indicated by the black boundary in Fig. 4 (c).

A total of 30 30 m × 30 m square sample plots were investigated in 2012. Zeng et al. (2022) provided thorough descriptions of these plots as well as plot measurements. Differential GPS was used to position and identify each plot. Diameter at breast height (DBH) that larger than 5 cm, height, and species information were recorded. Fig. 3 (b) shows the distribution of total and component AGB values for Genhe test site. In this study, the time intervals between the field campaigns and SAR data acquisitions at two test sites were considered through the growth conditions of dominated tree species. The AGB changes resulted from the time intervals were compensated by growth pattern models of the corresponding tree species introduced in Li et al. (1984), Zhang et al. (2008), and Wang et al. (2016).

3. Methodology

3.1. Measurement of field total and component forest AGB

AGB, which was named as "above-stump woody biomass" by forest resources assessment in 2000, is firstly defined as the mass of the woody part (stem, bark, branches, twigs) of trees, alive or dead, shrubs and bushes, excluding stumps and roots (Köhl et al., 2006). According to the definition of AGB from FAO, in this study, the forest components AGB included trunk (corresponding to stem), bark, branches, and leaves (corresponding to twigs). The direct assessment the AGB of a tree is done by a destructive process. However, as the assessment is destructive this method cannot be used for monitoring tree growth by permanent assessments. One alternative is to derive AGB functions with tree attributes such as diameters and tree height or crown attributes, moisture content, and wood density as independent predictors of AGB. Related researches began since 1990, previous studies developed distinguished allometric equations for AGB assessment of different tree species (Van and Akça, 2007). In order to determine AGB of each component of the entire tree, Valentine et al. (1984) compared randomized branch sampling (RBS) with the closely related importance sampling (IS) to obtain component AGB estimates of individual trees. Then several models had been proposed and used to estimate the forest AGB components and the total tree AGB from the tree characteristics. Many of these models are based on the assumed allometric relation between AGB and the tree or component characteristic. For example, Landis et al. (1975) regressed stem, bark, branch, and leaf biomass, as well as the total AGB. Mitchell et al. (1981) developed regression equations with stem, branch, and foliage biomass of conifers as target variables and DBH as predictor.

Table 2
Accuracies of allometry model used in this study.

AGB	R^2	MPE/%
Total AGB (M_A, kg)	*Pinus yunnanensis:0.9485*	*Pinus yunnanensis:6.30*
	Larix gmelinii:0.9690	*Larix gmelinii:3.80*
	Betula platyphylla:0.9550	*Betula platyphylla:4.46*
Stem AGB (M_S, kg)	*Pinus yunnanensis:0.9494*	*Pinus yunnanensis:5.71*
	Larix gmelinii:0.9701	*Larix gmelinii:3.99*
	Betula platyphylla:0.9545	*Betula platyphylla:4.60*
Bark AGB (M_B, kg)	*Pinus yunnanensis:0.8724*	*Pinus yunnanensis:8.08*
	Larix gmelinii:0.8817	*Larix gmelinii:6.98*
	Betula platyphylla:0.8678	*Betula platyphylla:8.35*
Branch AGB (M_{Br}, kg)	*Pinus yunnanensis:0.8395*	*Pinus yunnanensis:9.29*
	Larix gmelinii:0.8513	*Larix gmelinii:9.94*
	Betula platyphylla:0.9545	*Betula platyphylla:8.93*
Leaf AGB (M_L, kg)	*Pinus yunnanensis:0.6540*	*Pinus yunnanensis:13.98*
	Larix gmelinii:0.7439	*Larix gmelinii:10.08*
	Betula platyphylla:0.6311	*Betula platyphylla:14.49*

Table 3
Biomass information table in two study areas /(Mg/ha).

Test site	Biomass	Maximum value	Minimum value	Mean value	Mid-value
Yiliang Test site	Total AGB	98.40	17.60	46.62	43.16
	Stem AGB	54.92	9.43	26.16	25.13
	Bark AGB	10.50	2.02	4.93	4.22
	Branch AGB	23.63	4.32	11.14	10.12
	Leaf AGB	9.34	1.83	4.39	3.70
Genhe Test site	Total AGB	173.70	13.80	64.91	53.17
	Stem AGB	111.57	9.04	41.58	33.70
	Bark AGB	16.56	1.24	6.33	4.83
	Branch AGB	38.18	2.61	13.90	10.50
	Leaf AGB	7.38	0.56	3.01	2.40

The allometric equations for components AGB assessment of individual trees were developed and organized as a national standard in recent years in China (eq.1 and eq.2) (SFAC, 2014, 2016a, 2016b). They were applied in our field measurement for total and component forest AGB calculation at two test sites involved in this study. In the two test sites, the total AGB of each plot was calculated by sum of AGB of each individual tree (M_A), the AGB of each individual tree was calculated by diameter at breast height (DBH) and tree height (H) based on allometric equations according to tree species (eq. (1)). The AGBs of stem, bark, branch, and leaf of each individual tree was calculated by eq. (2) with different values for g_1,g_2, and g_3 according to tree species and different values for g according to the parts of each individual tree ($g = 1$ for stem,$g = g_1$ for bark,$g = g_2$ for branch, and $g = g_3$ for leaf). Each component AGB of each plot were calculated by the sum of corresponding component AGB of each individual tree in the plot. The collected 15 sample plots distributed in Xiaoshao branch are shown in Fig. 2 (c) as yellow points. The total and component forest AGB values of the 15 plots are given in Fig. 3 (a).

$$M_A = \mathrm{aDBH}^b H^c \quad (1)$$

Where a = 0.070231, b = 2.10329, and c = 0.41120 for *Pinus yunnanensis*, a = 0.06848, b = 2.01549, and c = 0.59145 for *Larix gmelinii*, and a = 0.06807, b = 2.10850, and c = 0.52019 for *Betula platyphylla*.

$$M = \frac{g}{1 + g_1 + g_2 + g_3} \times M_A \quad (2)$$

where $g_1 = 1.50018 DBH^{-0.27008} H^{-0.57857}$,$g_2 = 1.93610 DBH^{0.61425}$

$H^{-1.36341}$, $g_3 = 2.37294DBH^{0.43806}H^{-1.54081}$ for *Pinus yunnanensis*, $g_1 = 0.36742DBH^{0.19257}H^{-1.36274}$,$g_2 = 2.30634DBH^{0.72188}H^{-1.54081}$, $g_3 = 1.57804DBH^{0.19257}H^{-1.6274}$ for *Larix gmelinii*, $g_1 = 0.53498DBH^{0.09004}H^{-0.46520}$, $g_2 = 1.05167DBH^{0.66925}H^{-1.04662}$, $g_3 = 0.61793DBH^{0.17097}H^{-0.88182}$ g3 = 0.61793DBH0.17097H-0.88182 for *Betula platyphylla, respectively*.

Note that, the uncertainty of each allometric equation for each component may result in uncertainties in forest component AGB estimation results. Table 2 represents the allometric model-accuracies applied in this study, where R-squared (R^2) is the determination coefficient of the allometric growth model, and Maximum Permissible Error (MPE, %) is the maximum permissible error of the model. Table 3 summarized the statistical information of the field total and component AGBs calculated using allometric equations from (1) to (3) at the two test sites.

3.2. SAR data processing and feature extraction

The preprocessing of the acquired SAR images includes calibration, multi-look, and terrain correction. The calibration functions of GF-3 and ALOS-2 PALSAR-2 were provided by Ji et al. (2021), while for Radarsat-2 data, readers are referred to Zhang et al. (2018, 2017). Multi-looked factors with 4 × 2, 3 × 3, and 2 × 2 were applied for GF-3, ALOS-2 PALSAR-2, and Radarsat-2 data at range and azimuth direction, respectively. A target pixel size around 10 m was adopted for later terrain correction. The digital elevation model (DEM) utilized for terrain correction is SRTM. The terrain correction in this study includes three steps like polarization orientation angle (POA) changes correction, effective scattering area (ESA) changes correction, and angular variation effect (AVE) correction (Zhao et al., 2017). POA correction performed trough the compensation of covariance matrix (C) with matrix V through eq. (3):

$$C_{POAc} = VCV^T$$
$$V = \frac{1}{2}\begin{bmatrix} 1+\cos 2\partial & \sqrt{2}\sin 2\partial & 1-\cos 2\partial \\ -\sqrt{2}\sin 2\partial & 2\cos 2\partial & \sqrt{2}\sin 2\partial \\ 1-\cos 2\partial & -\sqrt{2}\sin 2\partial & 1+\cos 2\partial \end{bmatrix} \quad \partial = \frac{1}{2}\left[\tan^{-1}\left(\frac{-4Re\left(\left\langle (S_{HH}-S_{VV})S_{HV}^{*}\right\rangle\right)}{-\left\langle |S_{HH}-S_{VV}|^2\right\rangle + 4\left\langle |S_{HV}|^2\right\rangle}\right)+\pi\right] \tag{3}$$

where S_{HH},S_{VV}, and S_{HV} are elements of scattering matrix S. ESA correction is through the C_{POAc} matrix by $C_{ESAc} = C_{POAc}\cdot\cos\varphi$ computed, it is compensated by projection angle φ which is generated during geocoding procedure using the geocoding lookup tables between SAR and 30 m SRTM DEM coordinate systems. AVE correction is performed at last by eq. (2) through C_{ESAc} and correction coefficient matrix K:

$$C_{AVEc} = C_{ESAc} \odot K$$
$$\sigma_{\theta_{loc}} = \sigma\cdot k(n) = \left(\frac{\cos\theta_{ref}}{\cos\theta_{loc}}\right)^{n} \quad \mathrm{n} = \mathrm{argmin}\left\{abs\left[\left|\rho\left(\theta_{loc},\sigma_{\theta_{loc}}\right)\right|\right]\right\} \quad \mathrm{K} = \frac{1}{2}\begin{bmatrix} k(n_{HH}) & \sqrt{k(n_{HH}+n_{HV})} & \sqrt{k(n_{HH}+n_{VV})} \\ \sqrt{k(n_{HH}+n_{HV})} & k(n_{HV}) & \sqrt{k(n_{HV}+n_{VV})} \\ \sqrt{k(n_{HH}+n_{VV})} & \sqrt{k(n_{HH}+n_{VV})} & k(n_{VV}) \end{bmatrix} \tag{4}$$

where σ is the uncorrected backscattering coefficient;$k(n)$ is the correction coefficient; θ_{loc} is the local incidence angle;θ_{ref} is the reference incidence angle;n is the correction factor determined by minimum correlation between $\sigma_{\theta_{loc}}$ and θ_{loc} through function $\rho(\,)$.

The backscattering coefficient of a SAR image can reflect vegetation information and correlate with forest AGB if it is not saturated (Lal et al., 2021). Therefore, the back-scattering coefficients of HH, VV, HV and VH polarization channels are used in this study. In order to extract information, three incoherent target decomposition methods namely Yamaguchi 3-component decomposition, Freeman 2-component decomposition, and H/A/alpha decomposition were applied in this paper. In addition, decompositions are able to also extract coherent components can be used for AGB estimation (Zhang et al., 2015), therefore the TSVM coherent objective decomposition method was included. In this paper, 29 polarimetric characteristics (Table 4) and four backscatter coefficients were obtained and utilized.

Table 4
The extracted polarimetric features from acquired SAR data.

Decomposition Methods	Features
Yamaguchi 3-component	Yamaguchi3 volume scattering component (VSC) (Y3_Vol); Yamaguchi3 surface scattering component (SSC) (Y3_Odd); Yamaguchi3 dihedral scattering component (DSC) (Y3_Dbl);
Freeman 2 component	Freeman2 VSV (F2_Vol); Freeman2 SSV (F2_Grd);
H/A/alpha	Scattering angle (Alpha); Anisotropy (Anisotropy); Entropy (Entropy); Single Reflectance Eigenvalue Relative Difference (SERD); Relative Difference in Secondary Reflectance Eigenvalues (DERD) Shannon Entropy (SE); Strength component of Shannon's entropy (SEi); The angular component of the polarization of the Shannon entropy (SEp); Radar Vegetation Index (RVI);
TSVM	4 symmetric scattering parameters (T_alpha_s, T_alpha_s1, T_alpha_s2, T_alpha_s3); 4 target phase angle parameters (T_phi_s; T_phi_s1, T_phi_s2, T_phi_s3); 4 target azimuth parameters (T_psi, T_psi1, T_psi2, T_psi3); 4 elliptical azimuth parameters (T_tau_m, T_tau_m1, T_tau_m2, T_tau_m3)

3.3. Retrieval model via GA-SVR algorithm

Ji et al. (2021) originally applied the theory of GA-SVR for forest AGB inversion. SVR provides the benefit of employing limited training

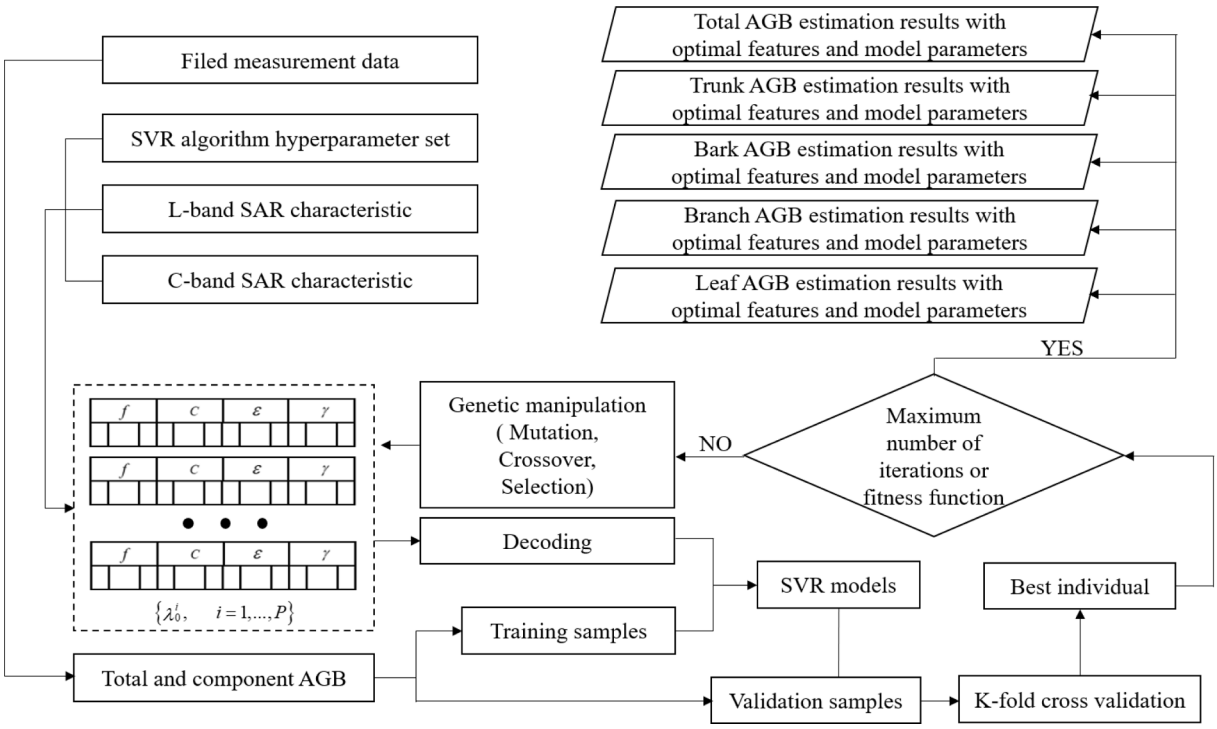

Fig. 5. Flowchart of the total and component AGB estimation via GA-SVR.

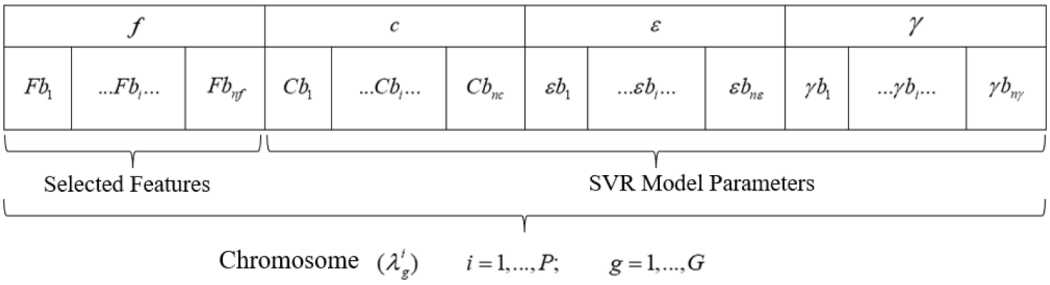

Fig. 6. Design of the chromosome.

samples to generate relatively high inversion accuracy and to address both nonlinear and linear issues. As a reason, it has grown more well-known and effective in forest AGB estimation (Bian, 2021; Geng, 2017; Gleason and Im, 2012). However, the selection of appropriate model parameters for the SVR is complicated limiting its usefulness. In recent year, GAs has been used for determining optimal SVR parameters showing improved performance (Haddadi et al., 2011; Whitley, 1994). In addition to SVR inversion model with its optimal GA-selected model parameters, identifying optimal polarimetric features is also a key for forest AGB estimation. GA-SVR algorithm used in this manuscript is able to optimize the input SAR features and SVR model hyperparameters simultaneously. Since identifying the optimal SAR features and selecting the SVR model hyperparameters are performed simultaneously, the chromosome of GA is designed by considering both SAR features and SVR model parameters. To design the chromosome of GA suitable for this study, in Fig. 5, SVR model parameters、SAR features are combined together as the input of GA-SVR models. The GA-SVR algorithms were used for the forest total and component AGB estimation. The flowchart of GA-SVR algorithms applied in this study are shown as Fig. 5.

The main steps of the GA-SVR algorithm include population initialization, fitness calculation, iteration and output of estimation results. During the population initialization, the chromosome of GA was constructed as shown in Fig. 6. 35 people were selected as the original population size. Following population initialization, a conventional SVR procedure is carried out utilizing the input training dataset, with the fitness function defined as $fitness = \left(1 - \frac{\sum_{i=1}^{K\times m} error}{K\times m} / AGB_{mean}\right) * 100$. It is conducted using a m repeated K-fold cross validation, $error$ represents an error metric such as root mean squared error (RMSE),AGB_{mean} is the mean value of field measured forest total and component AGBs. When the fitness function value meets the end constraint, the optimal features and model parameters become output and the cycle is stopped. If not, the next generation solution is generated using the mutation, crossover and selection operations set up in the process in Fig. 5, and the loop is stopped when the maximum number of iterations (200) is reached, outputting the best configuration of the inverse model. The output of the GA-SVR is the optimal SVR model hyperparameters, SAR features, and prediction data set.

3.4. Model validation

The model output validation is based on fieldwork recorded plot information and their corresponding SAR features predicted results using GA-SVR model. In this study, the leave one out cross validation (LOOCV) is used since the small samples in two test sites, LOOCV is a special example of K-fold cross validation is used for model training and

Table 5
Preferred set of GA parameters for each component of AGB estimation.

Test site	Biomass	Preferred parameters	Ratio
Yiliang	Total biomass	Y3_Dbl (C), HH (C), HV (C), SE (C), Y3_Vol (C), T_alpha_s1 (C), T_tau_m1 (C)	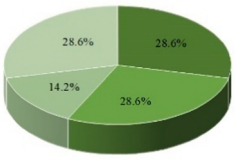
	Trunk biomass	Y3_Dbl (C), HH (C), HV (C), VV (C), SE (C), Y3_Vol (C), T_alpha_s1 (C)	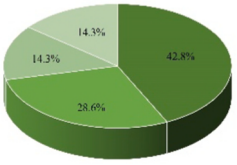
	Bark biomass	Y3_Vol (C), Y3_Dbl (C), HV (C), HH (C), SE (C), RVI (C), T_alpha_s1 (C)	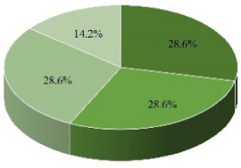
	Branch biomass	HV (C), HH (C), Y3_Vol (C), Y3_Dbl (C), SE (C), RVI (C), T_alpha_s1 (C)	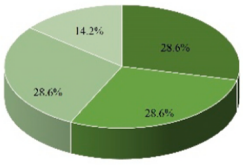
	Leaf biomass	HV (C), Y3_Vol (C), Y3_Dbl (C), SE (C), RVI (C), SERD (C), DERD (C)	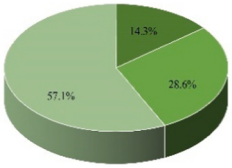
Genhe	Total biomass	Y3_Vol (C), T_tau_m2 (C), DERD (L), HH (C), HV (L), HV (C), SE (C), Y3_Dbl (C)	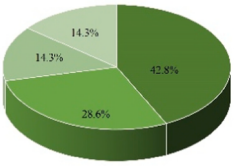
	Trunk biomass	T_tau_m2 (C), HH (C), HV (L), HH (L), SE (C), T_alpha_s1 (C), Y3_Vol (C), Y3_Dbl (L)	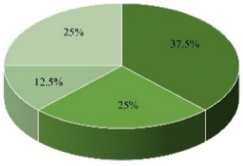
	Bark biomass	Y3_Vol (C), DERD (L), HV (L), HV (C), Y3_Dbl (C), SE (C), T_alpha_s1 (C)	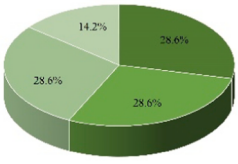
	Branch biomass	Y3_Vol (C), HV (L), VV (L), Y3_Dbl (C), SE (C), RVI (C), T_alpha_s1 (L)	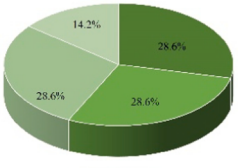
	Leaf biomass	Y3_Vol (C), DERD (L), HV (L), HV (C), Y3_Dbl (C), SE (C), T_psi_s1 (C)	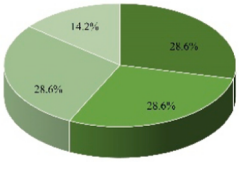

Note: (C) and (L) in the table indicate that the parameter was acquired from C-band or L-band data, respectively; Backscattering coefficient Yamaguchi 3-component decomposition The derived parameters TSVM decomposition.

validation. This method consists of dividing the initial dataset into K = 15 subsets for Yiliang test site and K = 30 subsets for Genhe test site and select K-1 to train the metamodel. The estimation error is then determined from the subset that is not utilized in the training process (Validation data). This procedure is repeated K times, each time with a different subset. The last RMSE value is derived by the mean of the K validated sample errors. Two methods were used for forest total and component AGB estimation validation. The first is to use 7 quantitative indices including the coefficient of determination R^2 (Eq (3), RMSE (Mg/ha, Eq (4), relative root mean square error (rRMSE, %, Eq (5), mean deviation (ME, Mg/ha, Eq (6)), mean absolute deviation (MAE, Mg/ha, Eq (7), mean percentage error (M%E, %, Eq (8), and mean absolute percentage error (MA%E, %, Eq (9) of the predicted results against the calculated AGB values through the field investigated plots (Wei et al. 2020). The second method uses scatterplots of the model estimated results and the real AGB values collected through the field campaign. The R^2 number, which varies from 0 to 1, shows the model's correctness; the closer it is to 1, the more accurate the model is, and vice versa; ME and M%E represent the sum and percentage of the difference between the predicted and measured values, through these two indicators, the overall underestimation of the model are qualified; RMSE and MAE are to access the discrepancy amid the anticipated and measured values, the smaller of these two indicators, the more accurate the model is; The smaller the values of these two indicators, the less the model deviates, rRMSE and MA%E show the percentage deviation and the degree of divergence between the anticipated and measured values.

$$R^2 = 1 - \frac{\sum_{i=1}^{n}(Y_i - y_i)^2}{\sum_{i=1}^{n}(Y_i - \bar{y})^2} \tag{5}$$

$$\mathrm{RMSE} = \sqrt{\frac{1}{n}\sum_{i=1}^{n}(Y_i - y_i)^2} \tag{6}$$

$$rRMSE = \frac{RMSE}{\bar{y}} \times 100\% \tag{7}$$

$$\mathrm{ME} = \sum_{i=1}^{n}\left(\frac{Y_i - y_i}{n}\right) \tag{8}$$

$$\mathrm{MAE} = \sum_{i=1}^{n}\left|\frac{Y_i - y_i}{n}\right| \tag{9}$$

$$\mathrm{M\%\ E} = \mathrm{E} = \frac{1}{n}\sum_{i=1}^{n}\left(\frac{Y_i - y_i}{Y_i}\right) \times 100\% \tag{10}$$

$$\mathrm{MA\%\ E} = \mathrm{E} = \frac{1}{n}\sum_{i=1}^{n}\left|\frac{Y_i - y_i}{Y_i}\right| \times 100\% \tag{11}$$

In the above equations, Y_i,y_i and $\bar{y}$ are the measured AGB of the *i-th* sample plot, the predicted AGB of the *i-th* sample plot, and the measured mean AGB, respectively, n is the sample plot numbers.

3.5. Forest total and component AGB inversion by GA-SVR

Since a SAR image pixel may be composed of multiple branches, leaves, barks, and trunks, it is difficult to justify which SAR features would be sensitive only to a particular forest component AGB, moreover, the sensitivity also affected by the penetration capability of microwave at different frequencies and the canopy density of the observed forest areas as well. In order to find the optimal features for forest total and component AGB estimation, regression models and machine learning methods were applied for feature optimization (Kasischke et al., 1995; Tsui et al., 2012; Zeng et al., 2022; Zhang et al., 2022). In this study, the developed machine learning method GA-SVR was utilized for both SAR feature optimization and model inversion. For total forest AGB and each component AGB inversion, all of the extracted SAR features were input in GA-SVR algorithms and the optimized SAR features and SVR model parameters were determined simultaneously for each single estimation procedure. With the procedure, optimized SAR features which performed better for branches, leaves, barks, and trunks AGB or forest total AGB estimation were selected and applied for their AGB estimations with the simultaneously optimized SVR parameters. Then the results were validated by the leave-one-out cross-validation method and described by equations from (5) to (11). In this study, five different GA-SVR algorithms were trained and validated for total, branches, leaves, barks, and trunks AGB estimation, respectively. With the performance of each GA-SVR algorithm, the optimal and more sensitive SAR features to different component AGB and total AGB were determined.

4. Retrieval results

Due to the statistical nature inherent to the suggested GA-SVR method, the inversion procedure was performed ten times for selecting the best polarimetric features and SVR model parameters and to estimate forest total and component AGB. The inversion operation was repeated several times in an effort to lessen randomization and enhance the stability of the inversion findings. In this study, the polarimetric features and SVR model parameters selected in best optimization procedure were kept and recorded. To compare the performance of GA-SVR, SVR algorithms were applied in forest total and component AGB estimation and their results were compared with GA-SVR estimated results according to 7 quantitative indices and scatter plots introduced in section 3.3.

4.1. Optimal predictive polarimetric SAR features

The feature selection showed distinct discrepancies at the two test sites when it comes to the relationship between polarimetric backscattering and models for estimating forest AGB variables. These differences are likely due to the diverse tree species that caused the various scattering processes. Since these differences were large it was evident that two models were needed and therefore the results reported here considered thus the best predictive polarimetric features dependent on test site, wavelength, and the levels of AGB. In the future, having a much larger dataset and including geographical location may reveal a solution, but for the moment, the model still needs to be training on some forest with common characteristics and it cannot be exported to type of forests that have not been seen before during training.

Table 3 showed the optimal predictive polarimetric SAR features selected by GA algorithm at C- and L- band in Yiliang and Genhe test sites for forest total and component AGB retrievals. The best predictive features in two test sites combined both backscattering coefficients at various polarimetric channels with a number of polarimetric decomposition parameters and their derived parameters. However, all the decomposition parameter extracted from Freeman-Durden decomposition methods did not occur in Table 3. This is because Yamaguchi 4 is showing very similar features with Freeman-Durden. Note that in Yiliang test site, C- band polarimetric SAR features provide better predictor for all forest AGB variables since all of the selected SAR features come from C- band. While a few polarimetric features from L- band were selected as best predictive features for forest AGB retrievals in Genhe test site. The phenomena might be caused by the distinct forest structure,

Table 6
Optimal hyperparameters selected for the GA-SVR algorithm at two test sites.

Study area	Penalty factor (c)	Width of Gaussian kernel function (γ)
Yiliang	200	0.015
Genhe	150	0.015

Table 7
Results of the estimated forest total AGB via GA-SVR.

Study area	R^2	RMSE (Mg/ha)	rRMSE (%)	ME (Mg/ha)	MAE (Mg/ha)	M%E (%)	MA%E (%)
Yiliang	0.679	14.43	30.96	0.23	12.32	0.50	26.43
Genhe	0.639	25.01	38.53	−1.99	19.79	−3.06	30.48

such as the varying average AGB levels at two test sites. The average forest AGB at Yiliang is lower than that at Genhe, meanwhile, individual trees are younger and the forest are thinner which make C- band showed better response to the forest AGB changes at Yiliang test site. Even in Genhe site, which has the higher average AGB level of 78 Mg/ha, the selected dominant polarimetric SAR features are from C- band as well.

The backscatter coefficients almost at each polarization channel were selected as optimal predictors for forest total and component AGB retrievals. Note that HV channel is shown as the only one optimal backscatter coefficient for leaf AGB estimation at both test sites. This finding confirmss the sensitivity of the HV channel to volume scattering, which is characteristic of forest canopies especially for leaf scattering. While for branches in forest canopies, HH at C- band is an optimal predictor at Yiliang test site and VV at L- band is at Genhe test site which show the dominant vertical or horizontal polarization scattering in branches. TSVM_alpha_s1 extracted from TSVM decomposition method in Table 3 represents an optimal predictor for almost all components and total AGB as well. It is the same to Yam3_Dbl and Yam3_Vol extracted from the Yamaguchi decomposition.

The ratio of the selected four types of polarimetric features by GA are shown in Table 5. The distribution of the four types of polarimetric features in the pie charts also revealed the distinguished scattering mechanisms at two test sites especially for total AGB and trunk AGB. Total AGB at Yiliang test site, has no optimal feature types, while at Genhe test site backscattering coefficients show as dominant in selected features. Differently than total AGB, the ratio of selected optimal feature ratios is similar for trunk AGB retrieval at the two test sites.

4.2. Forest total AGB retrieval

The GA-SVR algorithm used in this paper was implemented using the Python. The specific parameters of the algorithm used in the study were set as follows: for GA procedure, the selection method is tournament selection with an initial population size of 35; the maximum number of iterations is 200; the crossover method was single-point crossover with a crossover occurrence probability of 0.85; and the variation method is multi-point random variation with a variation occurrence probability of 0.25. The searching range of penalty (c) for SVR model parameter is set as 50, 100, 150, 200, 500, 1000, 1500, and 2000, respectively. While the values for width of Gaussian kernel function (γ) are 0.015, 0.02, 0.05, 0.1, 0.15, 0.2, 0.5, and 1.0, respectively.$m = 1$ is set in the fitness function for two test sites, while $K = 15$ is set for the Yiliang test site and $K = 30$ is set for the Genhe test site. With the iteration, the optimized two hyperparameters for SVR are summarized in Table 6 for forest total AGB estimating in the two test sites using GA-SVR algorithm (Table 7).

Performances of GA-SVR model for total AGB retrieval at Yiliang and Genhe test sites are presented in Table 6. Table 6 shows the R^2, RMSE, rRMSE, ME, MAE, M%E, and MA%E for two test sites. Scatterplots of observed and predicted forest total AGB for the two test sites are presented in Fig. 7 (a) and (b). According to quantitative parameters, GA-SVR models show better performance at the Yiliang test site compared to the Genhe test site. It has higher R^2 values with 0.679 compared $R^2 =$ 0.639 for Genhe test site. The RMSE values for two test sites are 14.43 Mg/ha and 25.01 Mg/ha, respectively. The rRMSE which describes random effects are 30.96% for Yiliang and 38.53% for Genhe. The ME and M%E show that there is a slight overall overestimation at Yiliang and some underestimation at Genhe. The scatterplots of Fig. 7 confirmed the results, the relationships between measured and predicted values in both test sites showed in Fig. 7 (a) and 7(b) are close to the 1:1 line, especially for points with ground measured AGB less than 80 Mg/ha in Fig. 7 (a) and points with AGB less than 100 Mg/ha in Fig. 7 (b). The scatterplots in Fig. 7 showed an obvious saturation for total forest AGB at two test sites, however, since only few plots showed the phenomenon of saturation, this needs further exploration in the future with more ground measurements.

To compare the reliability of the GA-SVR model in the two studies, we used the SVR model to estimate the forest total AGB in the two test sites. The SVR model is completed by the GridSearchCV function in the Sklearn Python library. The non-linear kernel function grid search

Table 8
Results of the estimated forest total AGB via SVR.

Study area	R^2	RMSE (Mg/ha)	rRMSE (%)	ME (Mg/ha)	MAE (Mg/ha)	M%E (%)	MA%E (%)
Yiliang	0.679	14.58	31.27	0.85	12.45	1.78	26.71
Genhe	0.635	25.23	38.86	−1.75	20	−2.7	30.81

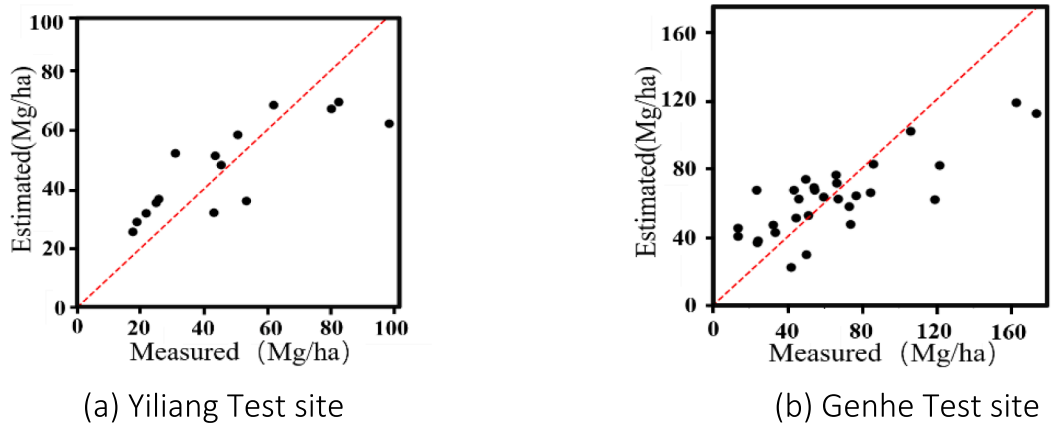

Fig. 7. Scatterplots of field measured versus GA-SVR estimated forest AGB.

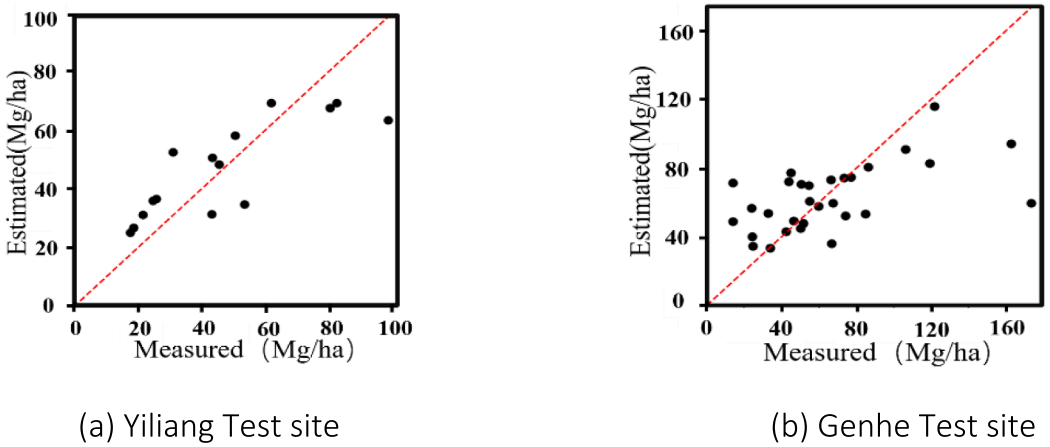

Fig. 8. Scatterplots of field measured versus SVR estimated forest AGB.

Table 9
The optimal hyperparameters selected for GA-SVR in two test sites.

Study area	Biomass	Penalty factor (c)	Width of Gaussian kernel function (γ)
Yiliang	Trunk	2000	0.015
	Bark	200	0.02
	Branch	1000	0.015
	Leaf	1000	0.015
Genhe	Trunk	2000	0.015
	Bark	1500	0.015
	Branch	1000	0.015
	Leaf	2000	0.015

optimization method is used for the SVR models, the results of SVR-retrieved total forest AGB were shown in Table 8 and Fig. 8.

In the Yiliang test site, although the coefficients of determination R^2 are the same for GA-SVR and SVR models, the error between the measured and predicted values using the GA-SVR model decreased when compared to SVR model. For instance, the values of ME and M%E, they were reduced 0.62 Mg/ha and 1.28%, respectively. In the Genhe test site, both ME and M%E were higher for GA-SVR model than the values acquired by SVR model. With the comparison of scatterplots using GA-SVR and SVR model at the two test sites, we found a slightly improvement of underestimation for the AGB predicted values when using GA-SVR model, especially when AGB levels at the Genhe test location are above 120 Mg/ha.

4.3. Forest component AGB retrieval

The optimized model parameters are presented in Table 9, the adjusted R^2, RMSE, rRMSE, ME, MAE, M%E, and MA%E for each model of two test sites are presented in Table 10.

GA-SVR model showed good performance for forest component AGB retrieval at both test sites with all R^2 values above 0.5. For the two test sites higher accuracy occurred for forest canopy AGB (branch component and leaf component) with respect to trunk AGB. For canopy AGB retrieval, all of the R^2 values were larger than 0.7 at Yiliang and higher than 0.6 at Genhe. While the R^2 values for trunk AGB at the Yiliang and Genhe test sites were 0.638 and 0.597, respectively. The rRMSE values in Table 8 and Table 5 also confirmed the decreased estimation accuracy for trunk component AGB than other components and total AGB. The values of ME and M%E of the Yiliang test site revealed overestimation of trunk component AGB with ME = 0.37 Mg/ha and M%E = 1.05%. While for other component AGB, slight underestimations were shown as well with ME values varying from −0.07 Mg/ha to −0.14 Mg/ha. In the Genhe test site, the underestimation phenomenon showed on all of the total and component AGB estimations with ME values varying from −0.15 Mg/ha to −1.99 Mg/ha and M%E values ranging from −1.43% to −3.94%.

Fig. 9 shows the retrieved forest components AGB using GA-SVR and optimal polarimetric features against ground measured plots. Each scatterplot displayed an agreement line (1:1 line) which represents the case when the predicted and field-collected values for the forest component AGB were identical. The estimated dynamic ranges for each component forest AGB at the Yiliang test site were are similar to the dynamic rangs of the field data. However, at Genhe, the dynamic range for the estimated trunk component is around 70 Mg/ha which is decreased compared with the 100 Mg/ha of the field collected data. The decreased dynamic range may result from the saturation of C- and L-band for trunk backscattering. Note that the estimated dynamic AGB ranges for other components at Genhe were similar to the corresponding measurements.

To better comprehend the efficacy of the GA-SVR approach, we also retrieved each component AGB using the SVR technique. The results for the SVR algorithm are detailed in Table 11 and Fig. 10. According to Table 11 and Fig. 10, the retrieval of forest components AGB is similar for SVR with GA-SVR but the GA-SVR outperforms SVR according to 7 quantitative parameters, namely R^2, RMSE, rRMSE, ME, MAE, M%E,

Table 10
Results of the estimated forest component AGBs via GA-SVR.

Study site	Biomass	R^2	RMSE (Mg/ha)	rRMSE (%)	ME (Mg/ha)	MAE (Mg/ha)	M%E (%)	MA%E (%)
Yiliang	Trunk	0.638	8.55	32.67	0.27	6.72	1.05	25.7
	Bark	0.727	1.27	25.72	−0.1	0.97	−2.11	19.6
	Branch	0.749	2.86	25.68	−0.14	1.98	−1.26	17.74
	Leaf	0.77	1.01	23.02	−0.07	0.81	−1.66	18.42
Genhe	Trunk	0.587	16.26	39.1	−0.6	13.14	−1.43	31.61
	Bark	0.669	2.19	34.52	−0.15	1.78	−2.39	28.13
	Branch	0.653	5.06	36.43	−0.25	1.83	−3.94	28.38
	Leaf	0.647	2.21	34.96	0.01	0.71	0.15	28.97

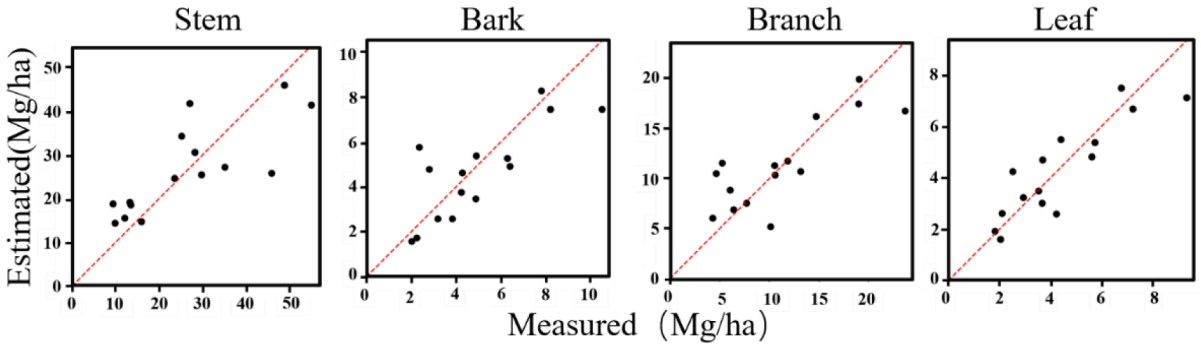

(a) Yiliang Test site

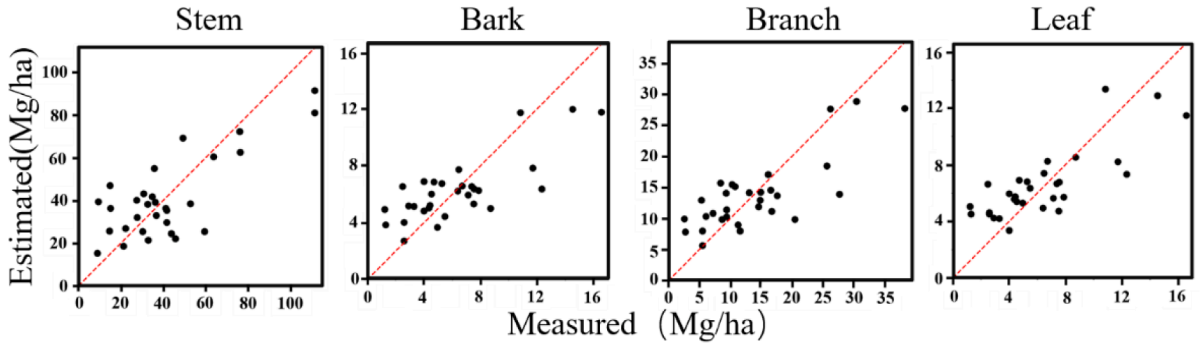

(b)Genhe Test site

Fig. 9. Scatterplots of field measured versus GA-SVR estimated forest component AGBs.

Table 11
Results of the estimated forest component AGBs via SVR.

Study area	Biomass	R^2	RMSE (Mg/ha)	rRMSE (%)	ME (Mg/ha)	MAE (Mg/ha)	M%E (%)	MA%E (%)
Yiliang	Trunk	0.621	8.81	33.66	0.48	7.04	1.84	26.91
	Bark	0.625	1.49	30.33	−0.28	1.17	−5.68	23.77
	Branch	0.697	3.05	26.11	0.3	2.44	2.51	20.93
	Leaf	0.712	1.14	25.91	0.14	0.9	3.24	20.54
Genhe	Trunk	0.585	16.29	39.18	−0.48	13.25	−1.14	31.86
	Bark	0.609	2.42	38.3	−0.04	1.97	−0.62	31.09
	Branch	0.62	5.33	38.33	−0.17	4.2	−1.24	30.25
	Leaf	0.638	2.32	36.71	0.26	1.94	4.04	30.64

and MA%E shown in Table 10. Moreover, SVR also showed better performance in Yiliang than Genhe, both for total and components AGB estimation. These results also reveal the higheraccuracy for canopy (leaf and branch) components compared to trunks with the lowest R^2 values (for Yiliang $R^2 = 0.621$ and for Genhe $R^2 = 0.585$) and highest rRMSE values (rRMSE = 33.66% for Yiliang and rRMSE = 38.33% for Genhe) in the two test sites. The scatterplot patterns in Fig. 10 displayed scattering modes that were comparable to those in Fig. 9, where a slight saturation phenomenon for trunk component AGB retrieval is present.

4.4. Exportability of models between the two test sites

In order to further explore the exportability of the proposed GA-SVR algorithm, the models were run for retrieval over the other tests site. Table 12 summarized the results. For the two test sites, a model constructed in Yiliang test site performed retrieval on Genhe test site (Validation test I)showing lower accuracy compared with models constructed in Genhe while validated over Yiliang (Validation test II). The exception is for leaf AGB estimation, where the better accuracy may result from the better sensitivity of C-band features to leaves. In section 4.1, we can see most of the polarimetric SAR features selected for total and component AGB estimation in the Yiliang test site are features from C-band SAR data. Other reason may be related to sample sizes. In Validation test I, only 15 samples in Yiliang are used for model-construction and training while 30 samples are used for validation. In Validation test II, 30 samples in Genhe are used for model-construction and training while 15 samples are used for validation. Moreover, the low cross-validation results with more rRMSE values greater than 50% in the two test sites may result in the difference of the selected optimized SAR polarimetric features in the two test sites. Only C-band features were selected in Yiliang test site while C- and L-band features were all involved in Genhe for total and component AGB estimations.

To further exploring the robustness of GA-SVR algorithm and its cross-site applicability, global forest AGB product derived from Global Ecosystem Dynamics Investigation (GEDI) (NASA, 2022) and China' forest AGB product derived by Aerospace Information Research Institute

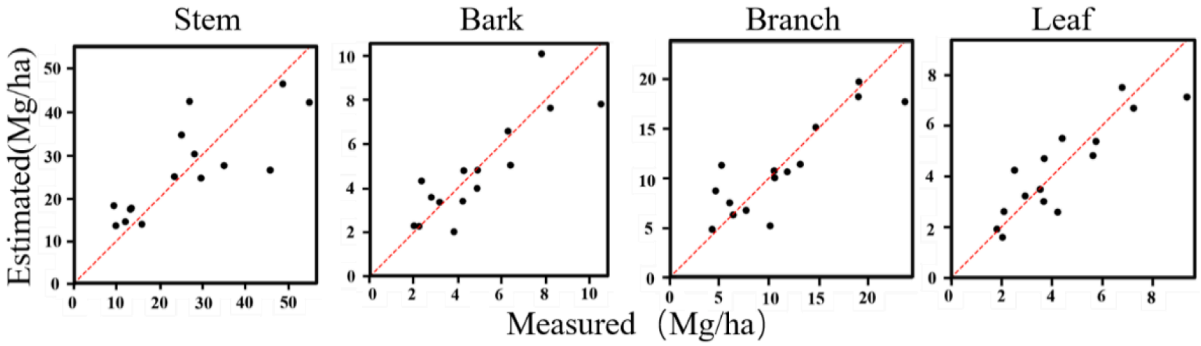

(a) Yiliang Test site

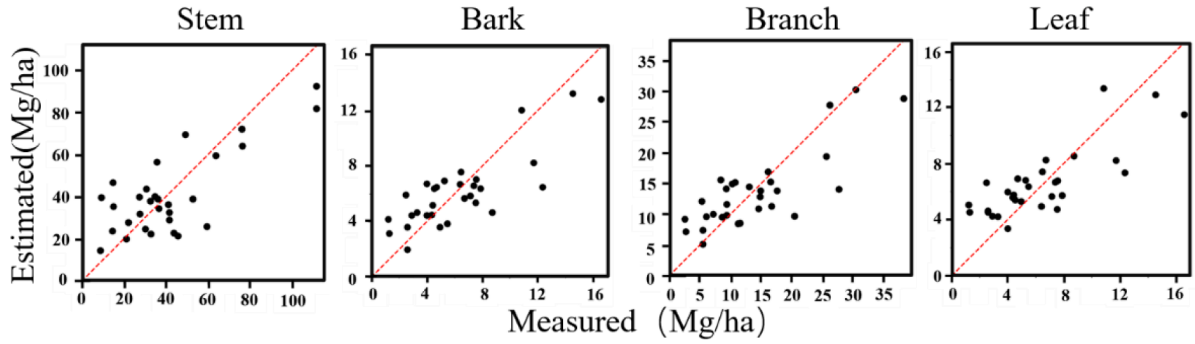

(b) Genhe Test site

Fig. 10. Scatterplots of field measured versus SVR estimated forest component AGBs.

Table 12
The results of the two study areas were cross-verified.

Model Building	Model Validation	AGB	R^2	RMSE (Mg/ha)	rRMSE / %	ME (Mg/ha)	MAE (Mg/ha)	M%E (%)	MA%E (%)
Yiliang	Genhe	Total	0.117	46.64	71.85	−26.29	32.90	−40.49	50.68
		Stem	0.189	30.27	72.82	−19.70	23.09	−47.39	55.54
		Bark	0.201	3.04	61.72	1.70	2.66	34.65	53.98
		Branch	0.153	6.61	59.4	2.76	5.70	24.74	51.20
		Leaf	0.118	2.29	50.23	−0.94	1.70	−21.51	38.84
Genhe	Yiliang	Total	0.180	22.40	48.05	1.02	19.07	2.19	40.90
		Stem	0.201	13.96	53.35	3.76	10.70	14.38	40.91
		Bark	0.149	2.60	52.87	1.71	2.27	23.77	46.14
		Branch	0.183	5.41	48.61	1.52	4.36	13.71	39.15
		Leaf	0.129	2.51	57.24	−1.56	1.81	−35.78	41.63

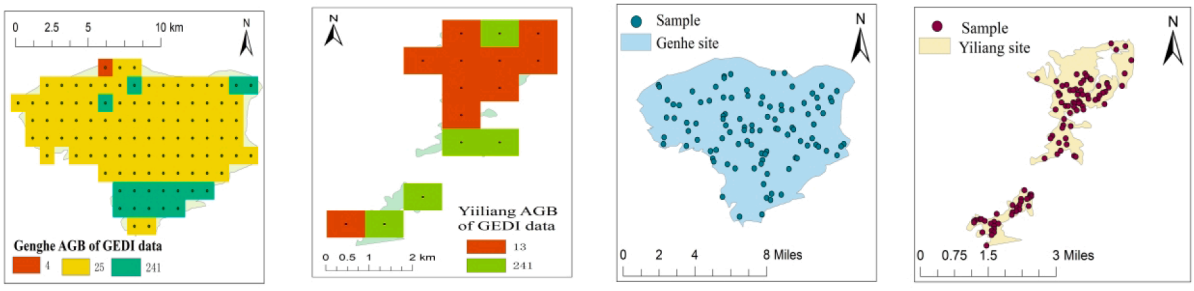

Genhe-GEDI Yiliang-GEDI Genhe-AIRI Yiliang-AIRI

Fig. 11. AGB point Distributions at two test sites from GEDI and AIRI products.

Table 13
The results of the two study areas were cross-verified using GEDI and AIRI products.

Data	Model Building	Model Validation	R^2	RMSE(Mg/ha)	rRMSE / %	ME (Mg/ha)	MAE (Mg/ha)	M%E (%)	MA%E (%)
GEDI	Yiliang	Genhe	0.15	74.83	122	−21.35	32.51	−1.11	1.69
	Genhe	Yiliang	0.29	90.60	102	−9.35	66.30	−0.11	0.75
30 m	Yiliang	Genhe	0.47	19.18	19.24	−2.58	13.97	−0.03	0.14
AGB	Genhe	Yiliang	0.29	25.18	20.06	−3.11	20.08	−0.02	0.16

(AIRI) (Yan et al., 2021) were applied in the two test sites for cross-validation. The resolution of AGB product from GEDI is 1 km, whereas that from AIRI is 30 m. Since only total AGBs are available of these products, here only total AGBs are used for model performance exploration and cross validation. For the GEDI AGB products at two test sites, all of the points in the two test sites are selected for model training and validation. Since the huge points of AIRI AGB product in the two test sites, 100 points at each test site were randomly selected and applied for GA-SVR model training and validation. Fig. 11 displays the spatial distributions of the points at two test sites with two AGB products. Table 13 summarized the performance of GA-SVR algorithms at two test sites and their cross-validation results.

The results from GEDI AGB products revealed a worse accuracy compared with that derived with AIRI product. It may result from the less range of AGB values in GEDI product. Since the coarse resolution and only 3 different AGB values at Genhe and two values at Yiliang, even there are more points located at two test sites, they are not enough to support GV-SVR for learning and training. In contrast, GA-SVR performed better using the AIRI AGB product. The RMSE values (19.18 Mg/ha and 25.18 Mg/ha) and rRMSE values (19.24% and 20.06%) with two-test validation even lower than that the models that were trained and validated at same test sites (14.58 Mg/ha and 31.27% for Yiliang; 25.23 Mg/ha and 38.86% for Genhe). The values of ME, MAE, M%E, and M% AE also revealed the transferable capability of GA-SVR especially with enough samples utilized for learning and training.

5. Discussion

5.1. Optimal selected polarimetric features

The GA algorithm in this study selected Yamaguchi3, TSVM decompositions, and backscattering coefficients as optimal input features for the retrievals of forest total and components AGB. Li et al. (2018) used the Bootstrap technique to select variables related to forest AGB in the Pangu forestry field of the Tahe Forestry Bureau in the northern foothills of the llghuli Mountains in the central Daxinganling. The nine optimal subsets selected included two TSVM polarization decomposition parameters indicating that the latter are sensitive to forest AGB, as confirmed in our study. Additionally several other authors showed that backscatter coefficients and Yamaguchi decomposition parameters were correlated to forest AGB (Golshani et al., 2019; Song and Fan, 2011; Wei et al., 2020; Zeng et al., 2022). Pan et al. (2020) used the KNN-SFS method to optimize the characteristic parameters of GF-3 PolSAR data, and their optimization results included the backscatter coefficients and various polarization decomposition parameters. Li et al. (2020)used random forest and KNN-FIFS methods to optimize the parameters of C-band SAR data in Genhe, and also found the backscatter coefficients and Yamaguchi decomposition correlated well with the forest AGB. In their study, the highest R^2 values between selected parameters and forest total AGB was 0.63.

Several selected optimal SAR polarimetric features used in a GA-SVR algorithm improved the correlation with total and component forest AGB in the two test sites compared with our previous studies (Zeng et al., 2022). The backscattering coefficient of the HV channel from C-band shows better performance in both test sites for forest total and component AGB estimation, on the other hand, the features extracted from L-band were only selected as optimal features in the Genhe test site. Additionally, the sensitivities of HV backscattering coefficients at C- and L-band to Loblolly pine forests were reported in the study of Kasischke et al., (1995). Volume scattering components (Y3_vol) and Shannon entropy (SE) extracted from C-band polarimetric SAR image were selected as optimal features both in two test sites for almost all of the component and total AGB retrievals. They also correlated well with total and component AGBs in the two test sites with all R values higher than 0.83 in Yiliang and 0.55 in Genhe. (Zeng et al., 2022). At Yiliang, the double-bounce component in C-band was useful for retrieving bark, branch and leave components AGB. This suggest that at Yiliang the double-bounce scattering mechanism at C-band may occurred between elements in the canopy, but not between the trunk and ground. At Genhe, the double-bounce component was selected at L-band for retrieving trunk AGB. This reveals the existence of expected double-bounce scattering between trunk and ground at L-band in Genhe. The good performance of polarimetric features extracted from the Yamaguchi decomposition corroborated its potential for describing forest vertical structure information (Cui et al.,2012). Only T_alpha_s1extracted from C-band were selected as optimal SAR features for forest total and component AGB estimation in the Yiliang. The results differed with the correlation analysis between SAR features and forest AGBs in Zeng et al., (2022), in which T_alpha_s1correlated lower compared with other features extracted by the TSVM decomposition.

5.2. Performance of GA-SVR algorithms

The GA-SVR algorithm were proposed and applied in forest AGB inversion by Ji et al. in 2021 for feature and model parameter optimization simultaneously. In their study, the performance of this algorithm was compared with the GA-SVR without SVR model parameter optimization but with feature optimization (GA + Default SVR) and GA-SVR with feature optimization using GA and SVR model parameter optimization using Grid searching (GA + Grid SVR). The outcomes demonstrated that GA-SVR utilized in this paper, which optimizes both characteristics and model parameters simultaneously, performs better than the other two GA-SVR algorithms. Here the GA-SVR were applied for forest total and component forest AGB estimation to explore its potential in component forest AGB estimations, and to assess how well it performs in comparison to the SVR algorithm. Few studies have investigated the retrieval of forest components AGB utilizing RS (Gao et al., 2018; Zhang et al., 2022). Comparison for different inversion algorithms, is really difficult when they are applied to diverse forests, using distinct RS data, and under various environment conditions. The good performance of GA-SVR in forest total AGB had been described in our previous study with better performance in Yiliang with C- band optimal polarimetric features compared to Genhe. Total and component forest AGB estimation using regression models revealed that adding C- and L-band SAR backscatter coefficients improved the inversion results where rRMSE values were improved about 6.5% for stem component and 17.9% for canopy component, respectively (Tsui et al., 2012). The total and component forest AGB in the Yiliang and Genhe test sites were inverted using the multiple linear stepwise regression method by Zeng et al. (2022), using the same SAR data as in this research. The results showed lower estimation accuracy, with R^2 ranges between 0.562 and 0.637 at Yiliang and 0.461 to 0.573 at Genhe. The findings of this study

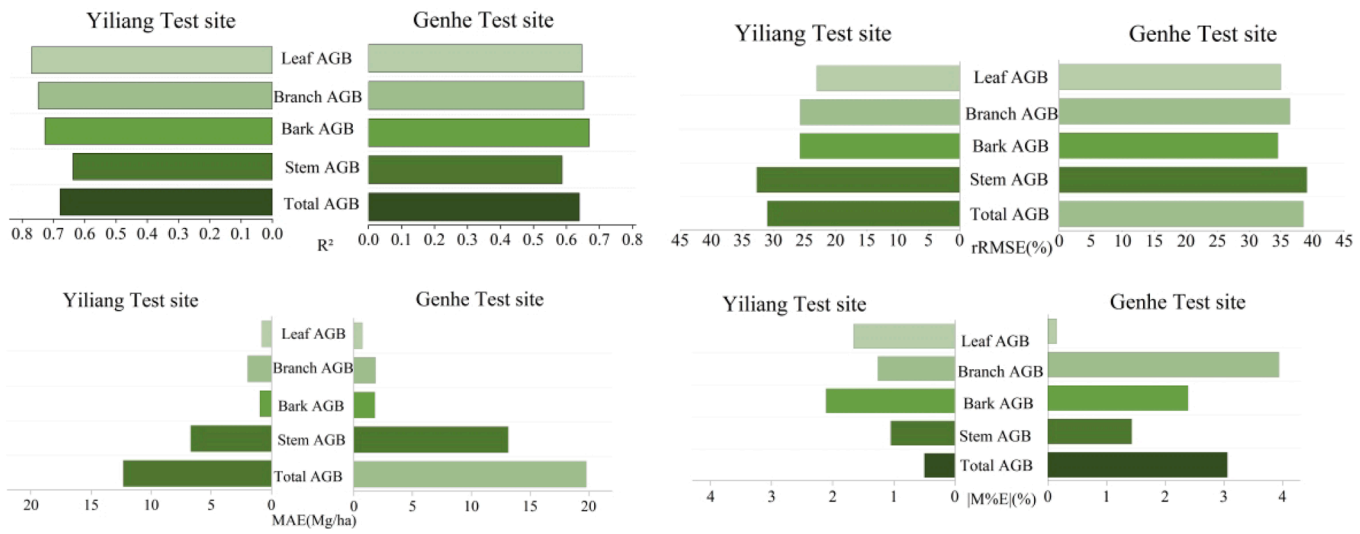

Fig. 12. Comparison of estimation results using GA-SVR algorithms in two test sites.

demonstrated the potential of GA-SVR used for component forest AGB inversion.

In order to test the robustness and transferability of GA-SVR algorithm optimizing RS feature and model parameter simultaneously, it was applied to the two test sites for AGB estimation with GEDI and AIRI AGB products as field measurements. Since the small AGB ranges of GEDI AGB product, the RMSE and rRMSE values are large. However, when AIRI AGB product with 100 points including large AGB ranges were applied in GA-SVR algorithms for two test site AGB estimation and their cross-validation as well, they acquired better performance even greater than that trained and validated in the same test site. Since Yiliang and Genhe represented quite different forest ecosystem and topography conditions, the results revealed the transferability of GA-SVR both for spatial and ecosystem. Note that, for the two test sites, a model constructed in Yiliang performed retrieval on Genhe(Validation test I) shows higher accuracy compared with models constructed in Genhe while validated over Yiliang (Validation test II). Considering the same samples (100) were selected in both test sites, the better performance at Validation test I may result from the large variation of topography in Yiliang, which made the learning and training procedure more representative and comprehensive. However, since only the SRTM DEM datasets were available for terrain correction the impact of topography remained after RTC correction was not considered in this study and the reason and the caused uncertainties need further explored in future when precise DEM is available.

5.3. Variability across test sites

Overall, the Genhe test site shows poor results than the Yiliang test site. It is unclear if this reflects different forest structure or particularities of topography of the two test sites. Yiliang has the most significant topographic variation compared to Genhe but the detailed terrain effects were corrected in this study using a three-step correction method (Zhao et al., 2017). Yunnan pines were the selected dominant tree species in Yiliang with lower forest AGB interval and average AGB values than Genhe. Despite the differences in GA-SVR performance between the two test sites, the rRMSE values obtained in this study were generally comparable between the two sites. For instance, the total forest AGB estimation results obtained by Cartus and Santoro with rRMSE values ranges from 19% to 45% (Cartus and Santoro, 2019), while in our study, they are 30.96% and 38.53%, respectively. Moreover, the component AGB especially for branch and leaf components estimation in this study all demonstrated no obvious saturation phenomenon.

The results of GA-SVR were further compared at the two experimental sites (Fig. 12). Fig. 12 confirmed that GA-SVR performed better for component forest AGB than the results of total AGB. For GA-SVR, the estimation accuracies of bark, branch and leaf AGB were higher than that of total AGB in both test sites. They revealed the estimation of component AGB may compensate the saturation problem occurred in total forest AGB estimation using SAR polarimetric features and GA-SVR algorithms.

6. Conclusions

The results presented and analyzed in this paper indicates that using the GA-SVR algorithm for total and component forest AGB estimation with C-, L-band polarimetric features including H/A/alpha, Freeman2, Yamaguchi3, and TSVM decompositions can provide reliable estimates. The best performance was obtained by using C- band features as model input on leaf and branch component AGB at Yiliang. While next better performance was obtained by using combination of C- and L-band features as input on leaf and branch component AGB estimation at Genhe. Above results confirmed the robustness of GA-SVR on component AGB estimation but they also suggested that the improvements that can be achieved depend on characteristics of the forest test site. Therefore, the models developed in a test site do not be expected to work in another test site where the forest structure is different. In the future we will investigate methodologies that can help exportability of models. Several features derived from the four decomposition methods were sensitive to forest total and component AGB. Polarimetric SAR features accompanied to GA-SVR offer a viable means for forest total and component AGB retrieval. With the availability of increased number of polarimetric SAR data at different frequencies, more frequency combination and polarimetric features need be further involved and explored in forest total and component AGB estimation.

Declaration of Competing Interest

The authors declare that they have no known competing financial interests or personal relationships that could have appeared to influence the work reported in this paper.

Data availability

The authors do not have permission to share data.

Acknowledgement

The authors would like to thank the European Space Agency for providing the polarimetric SAR data processing and educational tool box (PolSARpro) software and funding support from Agriculture Joint Special Project of Yunnan Province (Grant Number. 202301BD070001-058) and The National Natural Science Foundation of China (Grant Numbers: 32160365; 42161059; 31860240). Part of this work was done under the support of China Scholarship Council (CSC).

References

Astola, H., Häme, T., Sirro, L., Molinier, M., Kilpi, J., 2019. Comparison of Sentinel-2 and Landsat 8 imagery for forest variable prediction in boreal region. Remote Sens. Environ. 223, 257–273. https://doi.org/10.1016/j.rse.2019.01.019.

Avitabile, V., Herold, M., Heuvelink, G.B.M., Lewis, S.L., Phillips, O.L., Asner, G.P., Armston, J., Ashton, P.S., Banin, L., Bayol, N., Berry, N.J., Boeckx, P., Jong, B.H.J., DeVries, B., Girardin, C.A.J., Kearsley, E., Lindsell, J.A., Lopez-Gonzalez, G., Lucas, R., Malhi, Y., Morel, A., Mitchard, E.T.A., Nagy, L., Qie, L., Quinones, M.J., Ryan, C.M., Ferry, S.J.W., Sunderland, T., Laurin, G.V., Gatti, R.C., Valentini, R., Verbeeck, H., Wijaya, A., Willcock, S., 2016. An integrated pan-tropical biomass map using multiple reference datasets. Glob. Chang. Biol. 22, 1406–1420. https://doi.org/10.1111/gcb.13139.

Balzter, H., Luckman, A., Skinner, L., Rowland, C., Dawson, T., 2007. Observations of forest stand top height and mean height from interferometric SAR and LiDAR over a conifer plantation at Thetford Forest, UK. Int. J. Remote Sens. 28, 1173–1197. https://doi.org/10.1080/01431160600904998.

Banskota, A., Wynne, R.H., Johnson, P., Emessiene, B., 2011. Synergistic use of very high-frequency radar and discrete-return lidar for estimating biomass in temperate hardwood and mixed forests. Ann. For. Sci. 68, 347–356. https://doi.org/10.1007/s13595-011-0023-0.

Bian, R., 2021. Estimation of forest aboveground biomass in the Qilian Mountain National Park based on multi-source remote sensing data. Lanzhou University.

Blomberg, E., Ferro-Famil, L., Soja, M.J., Ulander, L.M.H., Tebaldini, S., 2018. Forest biomass retrieval from L-Band SAR using Tomographic ground backscatter removal. IEEE Geosci. Remote Sens. Lett. 15, 1030–1034. https://doi.org/10.1109/LGRS.2018.2819884.

Brovkina, O., Novotny, J., Cienciala, E., Zemek, F., Russ, R., 2017. Mapping forest aboveground biomass using airborne hyperspectral and LiDAR data in the mountainous conditions of Central Europe. Ecol. Eng. 100, 219–230. https://doi.org/10.1016/j.ecoleng.2016.12.004.

Cartus, O., Santoro, M., 2019. Exploring combinations of multi-temporal and multi-frequency radar backscatter observations to estimate above-ground biomass of tropical forest. Remote Sens. Environ. 232, 111313 https://doi.org/10.1016/j.rse.2019.111313.

Cartus, Santoro, Wegmüller, Rommen, 2019. Benchmarking the Retrieval of Biomass in Boreal Forests Using P-Band SAR Backscatter with Multi-Temporal C- and L-Band Observations. Remote Sensing 11, 1695. https://doi.org/10.3390/rs11141695.

Cazcarra-Bes, V., Tello-Alonso, M., Fischer, R., Heym, M., Papathanassiou, K., 2017. Monitoring of Forest Structure Dynamics by Means of L-Band SAR Tomography. Remote Sens. 9, 1229. https://doi.org/10.3390/rs9121229.

Chowdhury, T., Thiel, C., Schmullius, C., Stelmaszczuk-Górska, M., 2013. Polarimetric parameters for growing stock volume estimation using ALOS PALSAR L-band data over Siberian Forests. Remote Sens. 5, 5725–5756. https://doi.org/10.3390/rs5115725.

Cloude, S., 2009. Polarisation: Applications in Remote Sensing. Oxford Press.

Cloude, S.R., Papathanassiou, K.P., 1998. Polarimetric SAR Interferometry. IEEE Trans. Geosci. Remote Sens. 36 (5), 1551–1565.

Cloude, S.R., Papathanassiou, K.P., 2003. Three-Stage Inversion Process for Polarimetric SAR Interferometry. IEE Proceedings - Radar, Sonar and Navigation 150, 125–134.

Cui, Y., Yamaguchi, Y., Yang, J., Park, S.-E., Kobayashi, H., Singh, G., 2012. Three-component power decomposition for polarimetric SAR data based on adaptive volume scatter modeling. Remote Sens. 4, 1559–1572. https://doi.org/10.3390/rs4061559.

Duncanson, L., Kellner, J.R., Armston, J., et al., 2022. Aboveground biomass density models for NASA's Global Ecosystem Dynamics Investigation (GEDI) lidar mission. Remote Sens. Environ. 270, 112845 https://doi.org/10.1016/j.rse.2021.112845.

Englhart, S., Keuck, V., Siegert, F., 2011. Aboveground biomass retrieval in tropical forests — The potential of combined X- and L-band SAR data use. Remote Sens. Environ. 115, 1260–1271. https://doi.org/10.1016/j.rse.2011.01.008.

Gao, Y., Lu, D., Li, G., Wang, G., Chen, Q., Liu, L., Li, D., 2018. Comparative analysis of modeling algorithms for forest aboveground biomass estimation in a subtropical region. Remote Sens. 10, 627. https://doi.org/10.3390/rs10040627.

Garestier, F., Dubois-Fernandez, P.C., Guyon, D., Le Toan, T., 2009. Forest biophysical parameter estimation using L- and P-band polarimetric SAR data. IEEE Trans. Geosci. Remote Sens. 47, 3379–3388. https://doi.org/10.1109/TGRS.2009.2022947.

Geng, Q., 2017. Biomass estimation methods of Poplar Plantation based on multi source data. Nanjing Forestry University.

Gibbs, H.K., Brown, S., Niles, J.O., Foley, J.A., 2007. Monitoring and estimating tropical forest carbon stocks: making REDD a reality. Environ. Res. Lett. 2, 045023 https://doi.org/10.1088/1748-9326/2/4/045023.

Gleason, C.J., Im, J., 2012. Forest biomass estimation from airborne LiDAR data using machine learning approaches. Remote Sens. Environ. 125, 80–91. https://doi.org/10.1016/j.rse.2012.07.006.

Golshani, P., Maghsoudi, Y., Sohrabi, H., 2019. Relating ALOS-2 PALSAR-2 parameters to biomass and structure of Temperate broadleaf Hyrcanian forests. J. Indian Soc. Remote Sens. 47, 749–761. https://doi.org/10.1007/s12524-019-00948-0.

G. Haddadi A., Reza Sahebi, M., Mansourian, A., Polarimetric SAR feature selection using a genetic algorithm Canadian Journal of Remote Sensing 37 2011 27 36 10.5589/m11-013.

Hayashi, M., Motohka, T., Sawada, Y., 2019. Aboveground biomass mapping using ALOS-2/PALSAR-2 Time-Series images for Borneo's Forest. IEEE J. Sel. Top. Appl. Earth Obs. Remote Sens. 12, 5167–5177. https://doi.org/10.1109/JSTARS.2019.2957549.

Ji, Y., Xu, K., Zeng, P., Zhang, W., 2021. GA-SVR algorithm for improving forest above ground biomass estimation using SAR data. IEEE J. Sel. Top. Appl. Earth Observations Remote Sens. 14, 6585–6595. https://doi.org/10.1109/JSTARS.2021.3089151.

Kellndorfer, J., Walker, W., Pierce, L., Dobson, C., Fites, J.A., Hunsaker, C., Vona, J., Clutter, M., 2004. Vegetation height estimation from Shuttle Radar Topography Mission and National Elevation Datasets. Remote Sens. Environ. 93, 339–358. https://doi.org/10.1016/j.rse.2004.07.017.

M. Köhl S. Magnussen M. Marchetti Sampling methods, remote sensing and GIS multiresource forest inventory[M] 2006 Springer Heidelberg 10.1007/978-3-540-32572-7.

P. Lal A. Kumar P. Saikia A. Das C. Patnaik G. Kumar A.C. Pandey P. Srivastava C.S. Dwivedi M.L. Khan Effect of vegetation structure on above ground biomass in tropical deciduous forests of Central India Geocarto Int. 1–17 2021 10.1080/10106049.2021.1936213.

Lambert, M.C., Ung, C.H., Raulier, F., 2005. Canadian national tree aboveground biomass equations. Can. J. For. Res. 35, 1996–2018. https://doi.org/10.1139/x05-112.

Landis, T.D., 1975. Bolewood production and the environmental complex in the subalpine spruce/fir stands in SW Colorado. University of Colorado. Dissertation,.

Le Toan, T., Beaudoin, A., Riom, J., Guyon, D., 1992. Relating forest biomass to SAR data. IEEE Trans. Geosci. Remote Sens. 30, 403–411. https://doi.org/10.1109/36.134089.

Le Toan, T., Quegan, S., Davidson, M.W.J., Balzter, H., Paillou, P., Papathanassiou, K., Plummer, S., Rocca, F., Saatchi, S., Shugart, H., Ulander, L., 2011. The BIOMASS mission: Mapping global forest biomass to better understand the terrestrial carbon cycle. Remote Sens. Environ. 115, 2850–2860. https://doi.org/10.1016/j.rse.2011.03.020.

Li, B., Liu, Z., Wang, L., 1984. A primary study on the structure of the Forest Stands of Forest of Pinus Yunnanensis and the RegularPattern of its development. J. Yunnan Univ. 47–58.

Li, Y., Zhang, W., Cui, J., Li, C., Ji, Y., 2020. Inversion exploration on forest aboveground biomass of optical and SAR data supported by parameter optimization method. J. Beijing For. Univ. 42, 11–19. https://doi.org/10.12171/j.1000−1522.20190389.

Liao, Z., He, B., Quan, X., van Dijk, A.I.J.M., Qiu, S., Yin, C., 2019. Biomass estimation in dense tropical forest using multiple information from single-baseline P-band PolInSAR data. Remote Sens. Environ. 221, 489–507. https://doi.org/10.1016/j.rse.2018.11.027.

Lu, D., 2006. The potential and challenge of remote sensing-based biomass estimation. Int. J. Remote Sens. 27, 1297–1328. https://doi.org/10.1080/01431160500486732.

Lu, D., Chen, Q., Wang, G., Liu, L., Li, G., Moran, E., 2016. A survey of remote sensing-based aboveground biomass estimation methods in forest ecosystems. Int. J. Digit. Earth 9, 63–105. https://doi.org/10.1080/17538947.2014.990526.

Luckman, A., Baker, J., Kuplich, T.M., 1997. A study of the relationship between Radar baekseatter and regenerating Tropical Forest Biomass for Spaeeborne SAR Instruments. Remote Sens. Environ. 60, 1–13. https://doi.org/10.1016/S0034-4257(96)00121-6.

Mitchell, C.P., Proe, M.F., MacBrayne, C.G., 1981. Biomass tables for young conifer stands in Britain. KYOTO Biomass Studies 45–50.

NASA, ESDIS, 2022. Earthdata [WWW Document]. URL https://search.earthdata.nasa.gov/search.

Omar, H., Misman, M., Kassim, A., 2017. Synergetic of PALSAR-2 and Sentinel-1A SAR polarimetry for retrieving aboveground biomass in dipterocarp Forest of Malaysia. Appl. Sci. 7, 675. https://doi.org/10.3390/app7070675.

Pan, J., Xing, Y., Huang, J., Wang, X., 2020. Estimation of forest above-ground biomass based on GF-3 PolSAR data and Landsat-8 OLI data. J. Cent. Sounth Univ. For. Technol. 40, 83–90. https://doi.org/10.14067/j.cnki.1673-923x.2020.08.010.

Quegan, S., Le Toan, T., Chave, J., Dall, J., Exbrayat, J.-F., Minh, D.H.T., Lomas, M., D'Alessandro, M.M., Paillou, P., Papathanassiou, K., Rocca, F., Saatchi, S., Scipal, K., Shugart, H., Smallman, T.L., Soja, M.J., Tebaldini, S., Ulander, L., Villard, L., Williams, M., 2019. The European space agency BIOMASS mission: measuring forest above-ground biomass from space. Remote Sens. Environ. 227, 44–60. https://doi.org/10.1016/j.rse.2019.03.032.

Rosen, P.A., Kim, Y., Kumar, R., Misra, T., Bhan, R., Sagi, V.R., 2017. Global persistent SAR sampling with the NASA-ISRO SAR (NISAR) mission. In: in: 2017 IEEE Radar Conference (RadarConf). Presented at the 2017 IEEE Radar Conference (RadarConf17). IEEE, Seattle, WA, USA, pp. 0410–0414. https://doi.org/10.1109/RADAR.2017.7944237.

Sandberg, G., Ulander, L.M.H., Fransson, J.E.S., Holmgren, J., Le Toan, T., 2011. L- and P-band backscatter intensity for biomass retrieval in hemiboreal forest. Remote Sens. Environ. 115, 2874–2886. https://doi:10.1016/j.rse.2010.03.018.

Santi, E., Paloscia, S., Pettinato, S., Fontanelli, G., Mura, M., Zolli, C., Maselli, F., Chiesi, M., Bottai, L., Chirici, G., 2017. The potential of multifrequency SAR images

for estimating forest biomass in Mediterranean areas. Remote Sens. Environ. 200, 63–73. https://doi.org/10.1016/j.rse.2017.07.038.
Santoro, M., Askne, J., Smith, G., Fransson, J.E.S., 2002. Stem volume retrieval in boreal forests from ERS-1/2 interferometry. Remote Sens. Environ. 81, 19–35. https://doi.org/10.1016/S0034-4257(01)00329-7.
Santoro, M., Eriksson, L., Askne, J., Schmullius, C., 2006. Assessment of stand-wise stem volume retrieval in boreal forest from JERS-1 L-band SAR backscatter. Int. J. Remote Sens. 27, 3425–3454. https://doi.org/10.1080/01431160600646037.
Santoro, M., Fransson, J.E.S., Eriksson, L.E.B., Magnusson, M., Ulander, L.M.H., Olsson, H., 2009. Signatures of ALOS PALSAR L-band backscatter in Swedish Forest. IEEE Trans. Geosci. Remote Sens. 47, 4001–4019. https://doi.org/10.1109/TGRS.2009.2023906.
Song, Q., Fan, W., 2011. ALOS PALSAR estimation of vegetation biomass in Daxing'anling region. Chin. J. Appl. Ecol. 22, 303–308. https://doi.org/10.13287/j.1001-9332.2011.0074.
State Forestry Administration of China (SFAC) Tree Biomass Models and Related Parameters to Carbon Accounting for Pinus yunnanensis;State Forestry Administration of China 2014 Beijing, China 2 3 In Chinese.
State Forestry Administration of China (SFAC) Tree Biomass Models and Related Parameters to Carbon Accounting for Larix gmelinii; State Forestry Administration of China 2016 Beijing, China 2 6 In Chinese.
State Forestry Administration of China (SFAC) Tree Biomass Models and Related Parameters to Carbon Accounting for Betula platyphylla; State Forestry Administration of China 2016 Beijing, China 2 6 In Chinese.
Tebaldini, S., 2010. Single and Multipolarimetric SAR Tomography of Forested Areas: A Parametric Approach[J]. IEEE Trans. Geosci. Remote Sens. 48 (5), 2375–2387.
Tebaldini, S., Rocca, F., 2012. Multibaseline Polarimetric SAR Tomography of a Boreal Forest at P- and L-Bands[J]. IEEE Trans. Geosci. Remote Sens. 50 (1), 232–246. https://doi: 10.1109/TGRS.2011.2159614. https://doi: 10.1109/TGRS.2009.2037748.
Tsui, O.W., Coops, N.C., Wulder, M.A., Marshall, P.L., McCardle, A., 2012. Using multi-frequency radar and discrete-return LiDAR measurements to estimate above-ground biomass and biomass components in a coastal temperate forest. ISPRS J. Photogramm. Remote Sens. 69, 121–133. https://doi.org/10.1016/j.isprsjprs.2012.02.009.
Valentine, H.T., Tritton, L.M., Furnival, G.M., 1984. Subsampling trees for biomass, volume, or mineral content. For. Sci. 30 (3), 673–681. https://doi.org/10.1093/forestscience/30.3.673.
Van Laar, A., Akça, A., 2007. Forest mensuration. Springer Science & Business Media. https://doi.org/10.1007/978-1-4020-5991-9.
Wang, L., Wang, L., 2016. The Growth Model of DBH of Birch Based on Quantitative Theory. Anhui AgriSci.Bull 22, 89–99.
Wei, J., Fan, W., Yu, Y., Mao, X., 2020. Polarimetric decomposition parameters for artificial forest canopy biomass estimation using GF-3 fully polarimetric SAR data. Sci. Silvae Sincae 56, 174–183. https://doi.org/10.11707/j.1001-7488.20200919.
Whitley, D., 1994. A genetic algorithm tutorial. Stat. Comput. 4 https://doi.org/10.1007/BF00175354.
Xi, Z., Xu, H., Xing, Y., Gong, W., Chen, G., Yang, S., 2022. Forest canopy height mapping by synergizing ICESat-2, Sentinel-1, Sentinel-2 and Topographic information based on machine learning methods. Remote Sens. 14, 364. https://doi.org/10.3390/rs14020364.
Yan, S., He, G., Zhang, X. Forest aboveground biomass products in China, 2013-2021. https://doi.org/10.57760/sciencedb.07122.
Yu, Y., Saatchi, S., 2016. Sensitivity of L-band SAR backscatter to aboveground biomass of global forests. Remote Sens. 8, 522. https://doi.org/10.3390/rs8060522.
Yue H, Ferro-Famil L, Lardeux C. Polarimetric SAR tomography of tropical forests at P-BAND. 2011 IEEE International Geoscience and Remote Sensing Symposium, IGARSS 2011, Vancouver, BC, Canada, July 24-29, 2011. IEEE, 2011. https://doi: 10.1109/IGARSS.2011.6049321.
Zeng, P., Zhang, W., Li, Y., Shi, J., Wang, Z., 2022. Forest total and component above-ground biomass (AGB) estimation through C- and L-band polarimetric SAR Data. Forests 13, 442. https://doi.org/10.3390/f13030442.
Zhang, W., Li, Z., Chen, E., Zhang, Y., Yang, H., Zhao, L., Ji, Y., 2017. Compact polarimetric response of rape (Brassica napus L.) at C-Band: analysis and growth parameters inversion. Remote Sens. 9, 591. https://doi.org/10.3390/rs9060591.
Zhang, W., Chen, E., Li, Z., Zhao, L., Ji, Y., Zhang, Y., Liu, Z., 2018. Rape (Brassica napus L.) growth monitoring and mapping based on Radarsat-2 Time-Series data. Remote Sens. 10, 206. https://doi.org/10.3390/rs10020206.
H. Zhang C. Wang M. Liu LI, H., Shang, Z., Xie, L., Liu, Z., Polarisation SAR theory, methods and applications 2015 China Science Pulishing & Media Ltd Beijin.
Zhang, J., Sun, Y., Xu, J., 2008. Research on growing process of Larix gmeini Plantation in northeast of China. J. Northwest For. Univ. 23, 179–181.
Zhang, W., Zhao, L., Li, Y., Shi, J., Yan, M., Ji, Y., 2022. Forest above-ground biomass inversion using optical and SAR images based on a multi-step feature optimized inversion model. Remote Sens. 14, 1608. https://doi.org/10.3390/rs14071608.
Zhao, L., Chen, E., Li, Z., Zhang, W., Gu, X., 2017. Three-step semi-empirical radiometric terrain correction approach for PolSAR data applied to forested areas. Remote Sens. 9, 269. https://doi.org/10.3390/rs9030269.
Zhao, P., Lu, D., Wang, G., Wu, C., Huang, Y., Yu, S., 2016. Examining spectral reflectance saturation in Landsat imagery and corresponding solutions to improve forest aboveground biomass estimation. Remote Sens. 8, 469. https://doi.org/10.3390/rs8060469.